

RESEARCH ARTICLE

ZO-1 interactions with F-actin and occludin direct epithelial polarization and single lumen specification in 3D culture

Matthew A. Odenwald¹, Wangsun Choi^{2,*}, Aaron Buckley^{2,*}, Nitesh Shashikanth^{2,*}, Nora E. Joseph^{1,3,*}, Yitang Wang¹, Michael H. Warren¹, Mary M. Buschmann¹, Roman Pavlyuk², Jeffrey Hildebrand⁴, Ben Margolis⁵, Alan S. Fanning⁶ and Jerrold R. Turner^{1,2,7,†}

ABSTRACT

Epithelia within tubular organs form and expand lumens. Failure of these processes can result in serious developmental anomalies. Although tight junction assembly is crucial to epithelial polarization, the contribution of specific tight junction proteins to lumenogenesis is undefined. Here, we show that ZO-1 (also known as TJP1) is necessary for the formation of single lumens. Epithelia lacking this tight junction scaffolding protein form cysts with multiple lumens and are defective in the earliest phases of polarization, both in two and three dimensions. Expression of ZO-1 domain-deletion mutants demonstrated that the actin-binding region and U5-GuK domain are crucial to single lumen development. For actin-binding region, but not U5-GuK domain, mutants, this could be overcome by strong polarization cues from the extracellular matrix. Analysis of the U5-GuK binding partners shroom2, α -catenin and occludin showed that only occludin deletion led to multi-lumen cysts. Like ZO-1-deficiency, occludin deletion led to mitotic spindle orientation defects. Single lumen formation required the occludin OCEL domain, which binds to ZO-1. We conclude that ZO-1–occludin interactions regulate multiple phases of epithelial polarization by providing cell-intrinsic signals that are required for single lumen formation.

KEY WORDS: Cell polarity, Epithelial Cells, Tight junctions, Morphogenesis, Lumen Formation

INTRODUCTION

The ability to form and expand lumens is an essential characteristic of epithelia within tubular organs, such as kidneys and intestines, and is indispensable to their function. Such lumens are lined by a monolayer of intimately connected polarized epithelial cells in which apical surfaces face the lumen and basal membranes interface with the underlying basement membrane. Lumen formation can be modeled using Madin-Darby canine kidney (MDCK) cells embedded in extracellular-matrix-like gels. When a single cell suspension of MDCK cells is embedded in these gels, cells

proliferate and self-organize into well-polarized cysts containing a single hollow lumen.

Initial cues for epithelial polarization, relative to both the lumen and adjacent cells, occur through integrin-mediated signals from the extracellular matrix, which trigger directional membrane trafficking as early as the first cell division (Bryant et al., 2010; O'Brien et al., 2001; Yu et al., 2005b). The molecular composition of the extracellular matrix can determine both the rate of epithelial polarization and mechanism of lumen formation, but cellular machinery is also known to regulate lumen formation (Martín-Belmonte et al., 2008). The first sign of apical–basal polarization is the formation of the apical membrane initiation site (Bryant et al., 2010). This is followed by the formation of a pre-apical patch (PAP) that is demarcated by tight junctions and, through fluid accumulation and membrane repulsion, expansion to form a lumen (Bagnat et al., 2007; Bryant et al., 2010). Genesis of a single lumen requires coordination of polarized cell division (Hao et al., 2010; Jaffe et al., 2008; Qin et al., 2010), fluid accumulation (Bagnat et al., 2007), membrane delivery (Weis et al., 2016) and a balance between the kinetics of proliferation, apoptosis and polarization (Cerruti et al., 2013; Martín-Belmonte et al., 2008). These cellular processes are highly regulated and do not occur in isolation. For example, if another cell division occurs before the apical surface is defined through membrane trafficking, the apical membrane will be aberrantly placed and result in formation of multiple lumens. Indeed, some proteins known to orchestrate single lumen formation, such as Cdc42, have been implicated as key regulators of polarization, apical membrane trafficking and mitotic spindle orientation (Bryant et al., 2010; Jaffe et al., 2008; Martín-Belmonte et al., 2007, 2008).

The assembly of tight and adherens junctions at the edges of the pre-apical patch suggests that junctional proteins might be essential to cyst polarization. This is consistent with the placement of tight junctions at apicobasal interfaces in mature epithelial monolayers (Bryant et al., 2010) as well as with the association of many polarity proteins with the apical junctional complex and barrier development (Schluter et al., 2009; Shin et al., 2005; Straight et al., 2004). Tight junction proteins might, therefore, contribute to lumen formation. Although this has been studied to only a limited degree (Bagnat et al., 2007; Sourisseau et al., 2006; Tuncay et al., 2015), one report has demonstrated an essential role for claudin-15-mediated increases in paracellular permeability in lumen expansion (Bagnat et al., 2007). This is a well-understood process given that claudin-15 and related claudins form paracellular pores that conduct Na^+ (Amasheh et al., 2002; Colegio et al., 2002; Furuse et al., 2001; Van Itallie and Anderson, 2006; Weber et al., 2015). However, contributions of structural tight junction proteins that do not form conductance pathways, such as the intracellular scaffolding protein zonula occludens-1 (ZO-1; also known as TJP1) (Fanning and Anderson, 2009; Stevenson et al., 1986), have not been fully characterized.

¹Department of Pathology, The University of Chicago, Chicago, IL 60637, USA.

²Department of Medicine, Brigham and Women's Hospital and Harvard Medical School, Boston, MA 02115, USA. ³Department of Pathology, NorthShore University Health System, Evanston, IL 60201, USA. ⁴Department of Biological Sciences, University of Pittsburgh, Pittsburgh, PA 15260, USA. ⁵Department of Internal Medicine, University of Michigan, Ann Arbor, MI 48109, USA. ⁶Department of Cell Biology and Physiology, University of North Carolina, Chapel Hill, NC 27599, USA. ⁷Department of Pathology, Brigham and Women's Hospital and Harvard Medical School, Boston, MA 02115, USA.

*These authors contributed equally to this work

†Author for correspondence (jrtturner@bwh.harvard.edu)

© J.R.T., 0000-0003-0627-9455

ZO-1 is the founding member of the ZO family that also includes ZO-2 and ZO-3 (also known as TJP2 and TJP3, respectively). Each of these proteins contains multiple domains with numerous known and putative binding partners (Fanning and Anderson, 2009; Jesaitis and Goodenough, 1994; Stevenson et al., 1986; Van Itallie et al., 2013). Despite structural overlap, ZO-family proteins are functionally non-redundant, as demonstrated by the embryonic lethality of mice lacking either ZO-1 or ZO-2, but not ZO-3 (Katsuno et al., 2008; Xu et al., 2008). Although ZO-1 knockdown reduces the paracellular barrier to macromolecular flux and alters cortical actin organization, distinct apical and basolateral domains are well formed in ZO-1-deficient monolayers grown in two dimensions (Fanning et al., 2012; Ikenouchi et al., 2007; Rodgers et al., 2013; Umeda et al., 2006; Van Itallie et al., 2009). We hypothesized that growth in three dimensions, as occurs *in vivo*, might be a more demanding context that could reveal new ZO-1 functions. Herein, we show that ZO-1 is necessary for single lumen formation in three-dimensional (3D) cultures. Domain analysis reveals that ZO-1 U5-GuK-mediated interactions are particularly important for lumen formation. Of the known U5-GuK binding partners, only the transmembrane tight junction protein occludin is necessary for formation of a single lumen. Both ZO-1 and occludin regulate the orientation of cell division within epithelial cysts to control the formation of a single lumen. Occludin, but not occludin lacking the OCEL domain, which interacts with the ZO-1 U5-GuK domain, restored single lumen formation. These data show that ZO-1 acts as a cytosolic scaffold to orchestrate single lumen formation during 3D morphogenesis through direct interactions with occludin and the cytoskeleton.

RESULTS

ZO-1 is required for lumen morphogenesis

To assess the role of ZO-1 in epithelial morphogenesis, ZO-1-sufficient (WT) and ZO-1-knockdown (KD) MDCK cells were grown in 3D collagen gels (Fig. 1A). At 11 days after plating, >90% of WT cells had formed well-polarized epithelial monolayers surrounding single hollow lumens (Fig. 1B). As previously reported (Martín-Belmonte et al., 2008), many WT cysts displayed a multi-lumen phenotype at early time points that was progressively replaced by single lumen structures. In contrast, nearly half of ZO-1 KD cysts failed to form a discernable lumen within 4 days of plating (Fig. 1A,B). Lumens did eventually form, but most ZO-1 KD cysts had multiple lumens that persisted at day 11 (Fig. 1A,B). Some multi-lumen phenotypes observed in collagen gels are corrected by an extracellular matrix with strong external polarization cues, such as laminin-rich Matrigel (Lin et al., 1999; Martín-Belmonte et al., 2008). This did not, however, correct the multi-lumen phenotype of ZO-1 KD cysts (Fig. 1B,C).

Despite aberrant lumen development, single cell polarization was similar in mature cysts that had been generated from WT or KD cells; F-actin, podocalyxin (gp135; also known as PODXL) and atypical PKC ζ (aPKC ζ) were recruited to luminal surfaces, whereas E-cadherin localized to the lateral cell–cell contacts in mature cysts of both cell types (Fig. 1A,C; Fig. S1A). These data indicate that ZO-1 loss can be overcome to establish polarity within individual cells, but that ZO-1 is necessary for both morphogenesis and polarization at the tissue level.

ZO-1 is necessary for efficient epithelial polarization and barrier formation in 2D cultures

ZO-1 KD cells that had been grown in 3D culture displayed a striking multi-lumen phenotype typical of epithelia with polarization defects (Martín-Belmonte et al., 2008). Mature ZO-1 KD monolayers have

not, however, been reported to have polarization defects when grown in 2D culture (Fanning et al., 2012; Ikenouchi et al., 2007; Rodgers et al., 2013; Umeda et al., 2006; Van Itallie et al., 2009). We assessed polarization in 2D cultures by measuring protein localization and barrier development using a Ca²⁺-switch assay, which synchronizes the process. Upon Ca²⁺ repletion, WT monolayers developed trans-epithelial electrical resistance (TER), a measure of barrier function, in a manner characteristic of MDCK II cells. TER peaked within 12 h and then decreased to a steady state of <50 Ω *cm² within 36 h (Fig. 2A). In contrast, KD monolayers increased TER slowly and did not achieve a clear peak, although the ultimate steady-state TER was nearly identical to that of WT monolayers (Fig. 2A). This suggests that polarization and tight junction assembly are delayed in ZO-1 KD cells.

Expression and localization of occludin, aPKC ζ , the apical polarity protein PATJ and E-cadherin were also assessed. Expression of aPKC ζ and PATJ was stable during polarization and similar in WT and KD monolayers (Fig. 2B,C). In contrast, expression of occludin and E-cadherin, which bind to ZO-1 through direct and indirect interactions, respectively, were increased in KD monolayers, particularly during the first 24 h after Ca²⁺ repletion, when the TER of KD and WT monolayers was most different (Fig. 2A–C). Before Ca²⁺ repletion, PATJ and occludin were concentrated in intracellular pools, whereas E-cadherin formed a ring at the cell periphery in both WT and KD cells. Both occludin and PATJ were recruited to straight nascent tight junctions in WT monolayers within 1 h of Ca²⁺ repletion (Fig. 2D, yellow arrowheads). Within 3 h, these junctions developed undulations that were characteristic of MDCK II monolayers. In contrast, recruitment of both occludin and PATJ to the tight junction was retarded in KD monolayers (Fig. 2D,E). Although recruitment of both proteins increased over time, tight junctions remained straight, junctional occludin was discontinuous and cytoplasmic PATJ persisted in ZO-1 KD monolayers. In contrast, adherens junction assembly, as assessed by E-cadherin recruitment to basolateral cell–cell contacts, was similar in WT and KD monolayers (Fig. 2D,E). Because the quantitative morphometry analysis assessed the fraction of total fluorescence at the junction, these differences in recruitment were not due to differences in protein expression.

Proliferative imbalance contributes to the multi-lumen phenotype of ZO-1 KD cysts

ZO-1 has multiple potential functions that could result in multi-lumen cysts, including regulation of proliferation and apoptosis. These processes are crucial to lumen formation in cells grown in collagen gels, where polarization occurs slowly and multi-lumen intermediates resolve to single-lumen cysts through central cell apoptosis (Lin et al., 1999; Martín-Belmonte et al., 2008). We asked if these central cells might be resistant to apoptosis in ZO-1 KD cysts. However, apoptosis rates were low and similar in both WT and KD cysts at all developmental stages (Fig. S2A,B). We then considered the hypothesis that persistent proliferation might lead to multiple lumens in ZO-1 KD cysts. Consistent with this idea, ZO-1 KD cysts displayed higher proliferative rates than WT cysts at middle and late (e.g. days 8 and 11), but not early (e.g. day 4), times during cyst maturation (Fig. 3A,B). Morphological analyses indicated that, among the multi-lumen WT and KD cysts present at day 8, ~70% of proliferating cells were peripheral in WT cultures whereas only ~55% were peripheral (i.e. 45% were central) in KD cysts ($P < 0.05$; Fig. 3C). This balanced distribution of proliferating cells at peripheral and central sites of ZO-1 KD cysts persisted to at least 11 days post plating, but could not be assessed in WT cysts owing to the loss of central cells at later times. Importantly, the

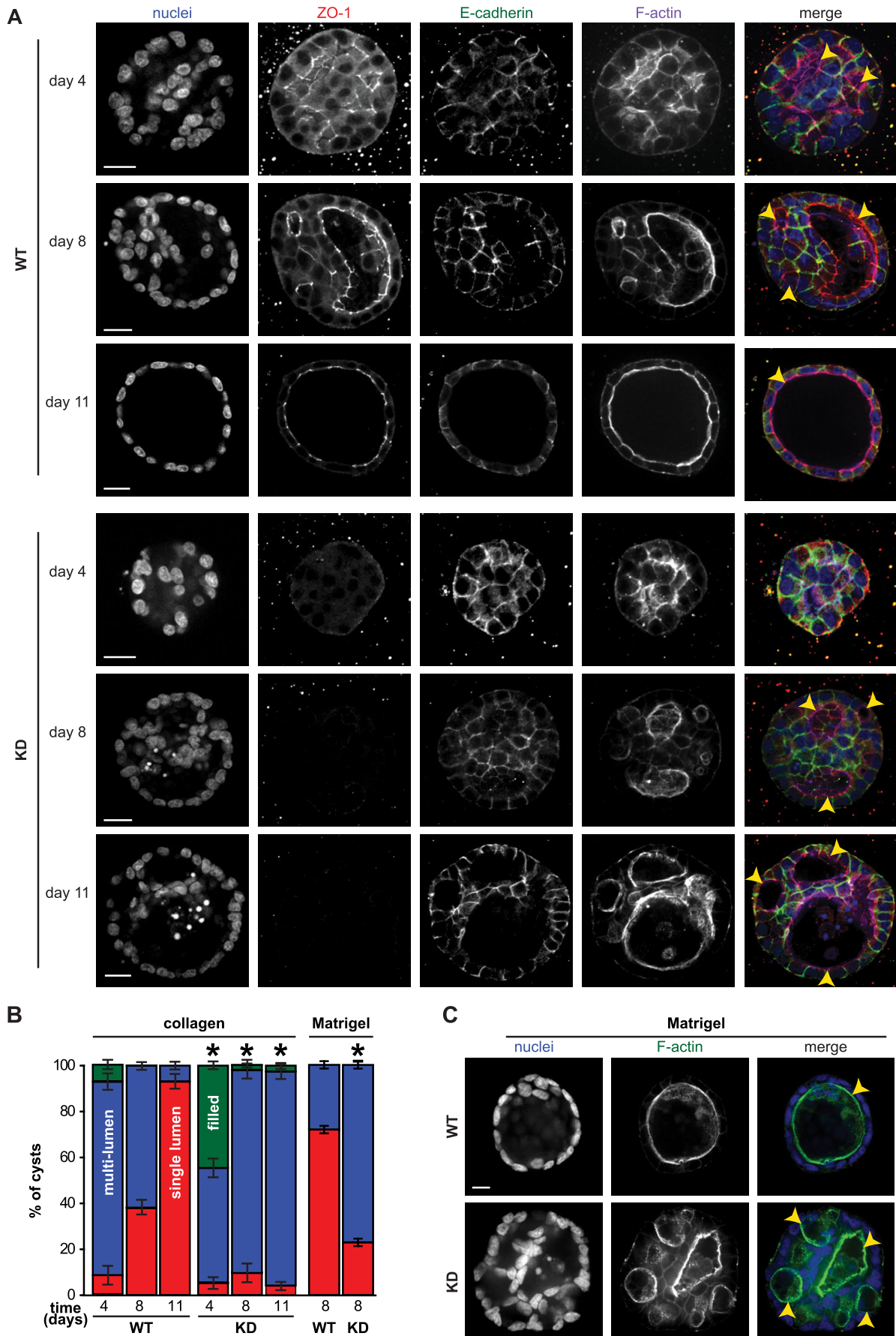


Fig. 1. See next page for legend.

Fig. 1. ZO-1 is required for lumen morphogenesis. (A) Representative images of WT and ZO-1 KD (KD) cysts stained for nuclei (blue, Hoechst 33342), ZO-1 (red), E-cadherin (green) and F-actin (phalloidin, purple) at days 4, 8 and 11 after plating in collagen gels. Yellow arrowheads indicate apical surfaces. Scale bars: 50 μm . (B) Lumen phenotypes at each time point in both growth conditions was classified as filled – i.e. no lumen (green) – multi-lumen (blue) or single lumen (red). Mean \pm s.e.m. of >100 cysts from at least three independent experiments with three or more samples per condition. * $P < 0.05$ by two-tailed t -test compared to WT. (C) Representative images of WT and KD cysts grown in Matrigel for 8 days; nuclei, blue, Hoechst 33342; F-actin, phalloidin, green. Yellow arrowheads indicate apical surfaces. Scale bar: 10 μm . Data are representative of at least three independent experiments with three or more samples for each condition, all with similar results.

multi-lumen phenotype and increased levels of proliferation were not due to a developmental delay in KD cysts, as extended growth (18 days) did not correct the multi-lumen phenotype and actually increased lumen number (Fig. S2C).

Consistent with increased proliferation of KD cells in 3D culture, growth curves of cells grown in two dimensions indicated that development of contact inhibition was delayed in ZO-1 KD cells, which continued to proliferate long after WT cells had achieved steady state cell densities (Fig. S2D). The enhanced proliferation of ZO-1 KD cells in 2D cultures could be abrogated by transfer to reduced serum (2.5% FBS) medium 4 days after plating (Fig. S2D). We applied the same approach to 3D cultures, reasoning that reducing concentrations of serum-derived growth factors would reduce proliferation in 3D cultures in a manner similar to that observed in 2D cultures. Consistent with this, replacement of medium containing 10% serum with medium containing only 2.5% serum at day 4 after plating more than doubled the number of single-lumen cysts in ZO-1 KD cell cultures (Fig. S2E). A smaller increase in the number of single-lumen cysts formed by WT cells was also seen after transfer to reduced serum medium. These data indicate that proliferative imbalance contributes to, but is not entirely responsible for, persistence of multiple lumens in ZO-1 KD cysts. The data also indicate that excessive growth stimulation could be a factor that contributes to the small number of multi-lumen cysts formed by WT cells.

ZO-1 depletion results in macromolecular barrier deficits in 3D culture

In contrast to cells grown in collagen gels, cells grown in Matrigel receive strong polarization cues, which trigger rapid development of a single lumen. The lumen then expands owing to fluid accumulation that partially depends on claudin-15, which forms paracellular Na^+ pores to establish an osmotic gradient and draw water into the lumen (Bagnat et al., 2007; Bryant and Mostov, 2008). In contrast to the size- and charge-selective paracellular pathway established by claudin-15 expression, relatively size-selective and charge-non-selective increases in paracellular flux are induced by ZO-1 KD (Fanning and Anderson, 2009; Fanning et al., 2012; McNeil et al., 2006; Van Itallie et al., 2009). Thus, although claudin-15 expression, which restores lumen formation, and ZO-1 KD, which induces multi-lumen formation, both increase paracellular permeability in 2D cultures, the size- and charge-selectivity of these changes differ. Notably, the MDCK II cells studied here express endogenous claudin-2, which forms a paracellular cation channel and dispenses with the requirement for claudin-15. To assess barrier function in 3D culture, cysts were loaded with small (Lucifer Yellow) and larger (3-kDa Texas-Red-Dextran) inert probes. Leak of both dyes from the lumen was significantly greater in ZO-1 KD, relative to WT, cysts (Fig. 3D), suggesting that, as reported in 2D cultures (Van Itallie et al., 2009),

ZO-1 KD increases paracellular permeability in 3D cultures in a relatively size-non-selective and charge-non-selective manner.

It is possible that the defective barrier of ZO-1 KD cysts limits the development of osmotic gradients that are necessary to sufficiently inflate a single lumen. We therefore hypothesized that ZO-1 KD cysts might contain a single collapsed lumen that only appears to be multiple lumens. To test this, cysts were perfused with hypotonic medium to induce luminal expansion (Fig. 3E). ZO-1 KD cysts displayed a small, but significant, increase in the rate of swelling, relative to WT, 20–40 min after initiation of hypotonic perfusion, consistent with the observed paracellular barrier deficits. After 120 min, however, the cross-sectional area of both WT and KD cyst lumens had increased to similar extents, to $\sim 300\%$ of the initial area. Further, interluminal septae in ZO-1 KD cysts persisted, indicating that the multi-lumen phenotype is not merely a consequence of an inadequately expanded single lumen. Consistent with this, ZO-1/ZO-2 double-KD cells, which have a more severe paracellular barrier phenotype than ZO-1 single KD cells (Rodgers et al., 2013; Spadaro et al., 2014; Van Itallie et al., 2009), formed single-lumen cysts (Fig. S1B–G). Further, ZO-2 expression within double-KD cells partially restored the multi-lumen phenotype of single ZO-1 KD cells (Fig. S1F,G).

Multiple ZO-1 domains contribute to the genesis of single-lumen cysts

Protein–protein interactions mediated by multiple ZO-1 domains contribute to tight junction assembly and barrier function (Fanning and Anderson, 2009). We therefore hypothesized that specific domains might be necessary for ZO-1 control over lumenogenesis. We tested this by expressing EGFP-tagged full-length and mutant ZO-1 in KD cells through an inducible promoter (Fig. S3A,B). EGFP alone had no effect on lumen generation in either collagen or Matrigel, whereas KD cells expressing full-length EGFP–ZO-1 formed well-polarized cysts with single lumens in both matrices (Fig. 4A,B). EGFP–ZO-1 lacking the actin binding region (ABR; EGFP–ZO-1 ^{Δ ABR}) (Fanning et al., 2002) was able to restore the single-lumen phenotype in Matrigel, but with reduced efficiency relative to full-length EGFP–ZO-1 (Fig. 4A,B; $P < 0.03$). In contrast, EGFP–ZO-1 ^{Δ ABR} was unable to restore single-lumen development when cells were grown in collagen gels (Fig. 4A,B), indicating that the ZO-1 ABR mediates morphogenetic processes that can be partially overcome by strong extracellular polarity cues.

Expression of EGFP–ZO-1 that lacked the U5-GuK domain (EGFP–ZO-1 ^{Δ U5-GuK}), which mediates interactions with multiple proteins, failed to correct the multi-lumen phenotype in either Matrigel or collagen (Fig. 4A,B). Moreover, 22% \pm 3% of EGFP–ZO-1 ^{Δ U5-GuK}-expressing cells formed solid spheres when grown in Matrigel (Fig. 4A,B). Immunostaining for claudin-1, occludin and ZO-2 in mature cysts revealed altered tight junction organization when comparing ZO-1 KD cells that expressed EGFP or EGFP–ZO-1 ^{Δ U5-GuK} to those expressing EGFP–ZO-1 or EGFP–ZO-1 ^{Δ ABR} (Fig. 4C). Although claudin-1 and occludin were recruited to tight junctions and basolateral membranes in cysts that expressed EGFP–ZO-1 or EGFP–ZO-1 ^{Δ ABR}, recruitment of both claudin-1 and occludin was deficient in cysts that expressed EGFP or EGFP–ZO-1 ^{Δ U5-GuK} (Fig. 4C). ZO-2 colocalized with all forms of ZO-1, including EGFP–ZO-1 ^{Δ U5-GuK} aggregates, but was diffusely distributed in ZO-1 KD cysts that expressed only EGFP (Fig. 4C). In contrast, neither ZO-1 KD nor expression of full-length or mutant forms had marked effects on the distribution of aPKC λ , gp135 or α -catenin in mature cysts (Fig. 4C). These data indicate that interactions mediated by the U5-GuK domain of ZO-1 are

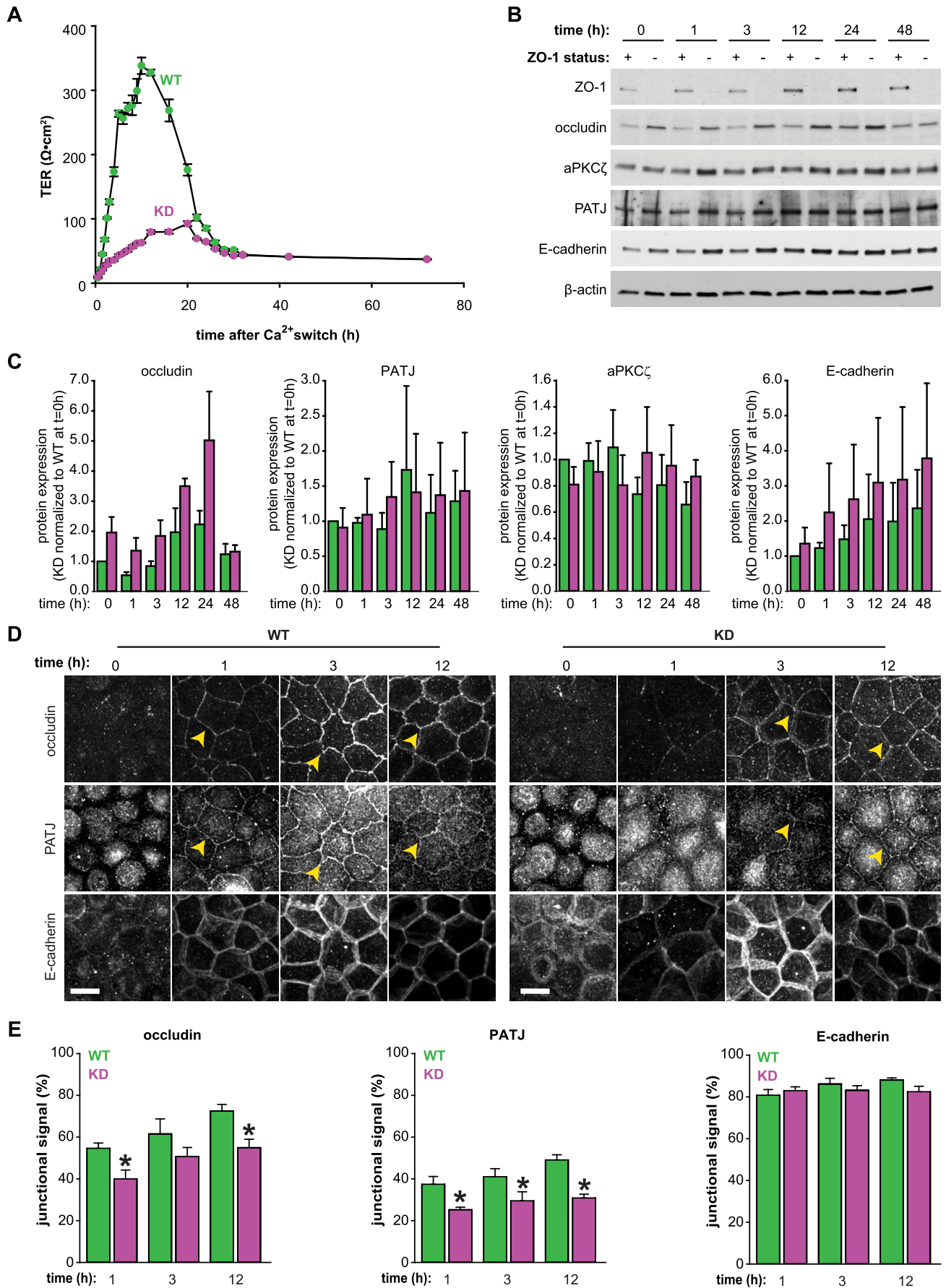


Fig. 2. See next page for legend.

Fig. 2. ZO-1 is necessary for efficient epithelial polarization and barrier formation in 2D cultures. (A) Development of TER after Ca^{2+} repletion in WT and ZO-1 KD (KD) cells. Mean \pm s.e.m. from one experiment representative of three similar studies, each performed in triplicate. (B) Immunoblotting analysis at the indicated times after Ca^{2+} repletion showing ZO-1, occludin, aPKC λ , PATJ, E-cadherin and β -actin. Results are representative of three independent experiments. (C) Densitometry analysis of immunoblots at the indicated time points. Mean \pm s.e.m. normalized to WT levels at 0 h. $P < 0.05$ for KD versus WT over the entire time course, for both occludin and E-cadherin expression, by Mann–Whitney U test. (D) Occludin, PATJ and E-cadherin distributions at the indicated times after Ca^{2+} repletion. Maximal projections of full-thickness z-stacks are shown. Yellow arrowheads indicate protein recruited to tight junctions. Scale bars: 10 μm . Data are representative of three independent experiments, all with similar results. (E) The percentage of the total fluorescence intensity that was found at cell–cell junctions was quantified in five cells per sample. Mean \pm s.e.m. for three independent experiments, each performed in triplicate. * $P < 0.05$ by paired two-tailed *t*-test comparing WT to KD at the indicated time points.

particularly crucial in orchestrating tight junction organization and lumen formation in 3D cultures, whereas effects on polarity and apical or basolateral proteins – i.e. aPKC λ , gp135 and α -catenin, respectively – were limited. The contrasting effects of ABR- and U5-GuK-deletion mutants on cyst development further indicate that the protein interactions mediated by these domains have distinct functions during epithelial organogenesis.

ZO-1 U5-GuK-domain-mediated interactions are necessary for epithelial polarization and paracellular barrier function in 2D culture

To better define the contributions of the ABR and U5-GuK domains to epithelial polarization, we returned to 2D Ca^{2+} -switch assays. When cultured in doxycycline, each line developed TER in a manner similar to the parental ZO-1 KD cells (Fig. S3C), confirming that the monolayers were similar to one another in the absence of ZO-1 expression. Induction of free EGFP expression had no effect on barrier development (Fig. S3C). Expression of either full-length EGFP–ZO-1 or EGFP–ZO-1 Δ ABR increased the peak TER, although this was 20% \pm 1.0% greater in monolayers that expressed full-length EGFP–ZO-1 relative to those expressing EGFP–ZO-1 Δ ABR. This suggests that ABR-mediated interactions play a role in initial barrier formation, consistent with their established role in barrier regulation (Yu et al., 2010). In contrast, induction of EGFP–ZO-1 Δ U5-GuK expression reduced the TER relative to that in uninduced controls (Fig. S3C).

In 2D cultures, free EGFP diffused throughout the cytoplasm, EGFP-tagged full-length ZO-1 and EGFP–ZO-1 Δ ABR were concentrated at tight junctions, and EGFP–ZO-1 Δ U5-GuK was located at tight junctions and in discrete cytoplasmic punctae (Fig. 5). EGFP–ZO-1 Δ U5-GuK expression markedly enhanced ZO-2 recruitment to tight junctions (Fig. S3D), but the distributions of occludin, claudin-1 and α -catenin were unaffected in mature monolayers (Fig. S3D). ZO-2 recruitment in monolayers that expressed EGFP-tagged full-length ZO-1 or EGFP–ZO-1 Δ ABR was similar to that in ZO-1 KD cells (Fig. S3D).

Consistent with the observed effects on TER development, morphological features of tight junction assembly were accelerated through expression of either full-length EGFP–ZO-1 or EGFP–ZO-1 Δ ABR in ZO-1 KD monolayers, with occludin and PATJ recruitment to nascent tight junctions detected within 1 h of Ca^{2+} repletion (Fig. 5; Table S1). In contrast, occludin and PATJ recruitment was not apparent until 3 h after Ca^{2+} repletion in monolayers that expressed free EGFP and were further depressed in monolayers that expressed EGFP–ZO-1 Δ U5-GuK (Fig. 5; Table S1). When considering

the heterogeneity in EGFP–ZO-1 Δ U5-GuK expression throughout the monolayer, it became clear that the degree to which occludin and PATJ recruitment was inhibited correlated directly with the extent of EGFP–ZO-1 Δ U5-GuK expression (Fig. 5, red arrows). ZO-1 Δ U5-GuK therefore disrupts tight junction assembly in a concentration-dependent manner. As a whole, these 2D and the preceding 3D culture data indicate that the U5-GuK region plays an essential role in epithelial polarization and barrier development, consistent with previous studies in 2D culture (Fanning et al., 2007; Ikenouchi et al., 2007; Rodgers et al., 2013). We also report the new finding that expression of ZO-1 that lacks U5-GuK enhances ZO-2 recruitment.

ZO-1 U5-GuK domain binding partners contribute uniquely to epithelial polarization

Given the importance of the ZO-1 U5-GuK domain demonstrated above, we asked whether one of the known U5-GuK binding partners was essential for epithelial polarization. The U5-GuK region interacts directly with the actin-binding protein shroom2, the adherens junction protein α -catenin and the transmembrane tight junction protein occludin (Etournay et al., 2007; Furuse et al., 1994; Itoh et al., 1997). Stable MDCK lines with knockdown of each of these proteins were assessed by using the Ca^{2+} -switch assay (Fig. 6A–C; Fig. S4A,B). Despite the known ability of shroom2 to regulate cortical actin through Rho kinase isoforms (ROCK), and the established roles of Rho kinases in cyst formation and actomyosin in barrier function (Dietz et al., 2006; Hartsock and Nelson, 2008; Madara et al., 1986; Yu et al., 2008), shroom2 knockdown had no effect on TER development after Ca^{2+} switch (Fig. 6B; Fig. S4A). Moreover, E-cadherin, ZO-1 and PATJ were all prominently localized to cell–cell junctions within 1 h of Ca^{2+} repletion (Fig. 6C; Fig. S4B, Table S2).

α -catenin regulates both tight junction development and ZO-1 recruitment to tight junctions and, therefore, might also regulate epithelial organization (Capaldo and Macara, 2007; Maiers et al., 2013). Cells lacking α -catenin (Fig. 6A) were easily detected in subconfluent cultures owing to their elongated profiles, but were morphologically indistinguishable from WT cells when grown to confluence on 2D supports (Fig. 6C; Fig. S4B), although the peak TER was reduced over 50% relative to that of WT monolayers (Fig. 6B; Fig. S4A). Development of TER was also delayed in α -catenin KD monolayers, and this correlated with retarded recruitment of E-cadherin, occludin and PATJ to junctions (Fig. 6C; Fig. S4B, Table S2). Notably, PATJ and ZO-1 were not recruited to tight junctions of α -catenin-deficient cells until 12 h after Ca^{2+} repletion (Fig. 6C; Fig. S4B).

Occludin KD monolayers (Fig. 6A) were also subjected to Ca^{2+} switch and exhibited an approximately 50% reduction in peak TER relative to WT controls (Fig. 6B; Fig. S4A). However, PATJ and ZO-1 were recruited to the tight junctions of occludin-deficient monolayers with an efficiency similar to that in WT monolayers (Fig. 6C; Fig. S4B, Table S2). Taken together, these data indicate that occludin and α -catenin, but not shroom2, contribute significantly to structural and functional polarization of epithelial monolayers in 2D culture.

The U5-GuK binding partner occludin, but not α -catenin or shroom2, is necessary for the formation of single-lumen cysts

We next assessed the ability of occludin-, α -catenin- and shroom2-deficient cells to form single-lumen cysts in 3D culture. Shroom2-deficient MDCK cells formed polarized single-lumen cysts when grown in either collagen or Matrigel (Fig. 6D), consistent with the

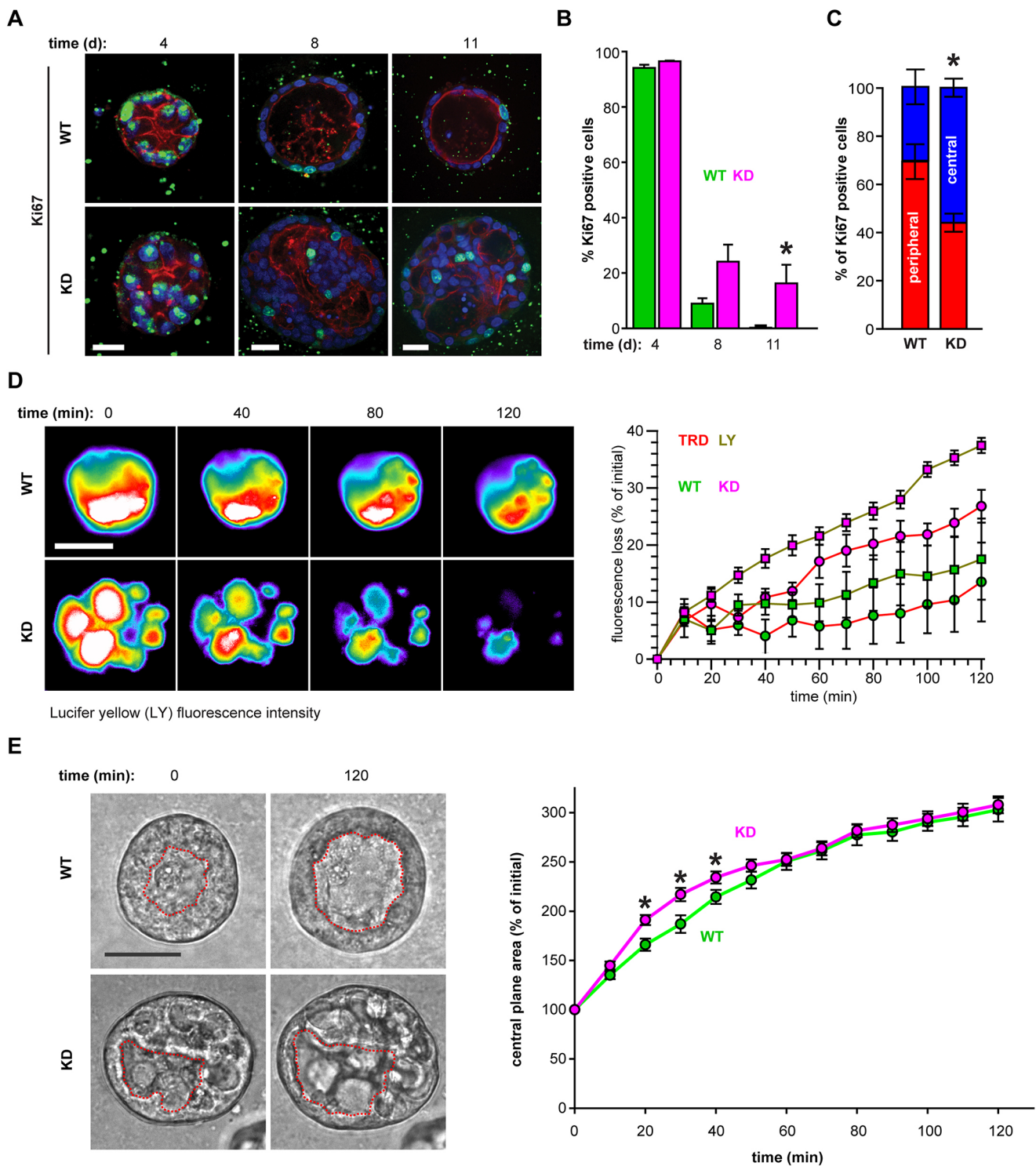


Fig. 3. ZO-1 regulates epithelial proliferation and the macromolecular barrier in 3D structures. (A) Representative images of WT and ZO-1 KD (KD) cysts grown in collagen and stained for Ki67 (green), nuclei (blue, Hoechst 33342) and F-actin (red, phalloidin) at the indicated times. Scale bars: 10 μ m. (B) The percentage of cells positive for Ki67. Ten cysts were scored for each condition in each of three independent experiments. Mean \pm s.e.m. of three independent experiments, each performed in triplicate. * P <0.05 by two-tailed t -test compared to WT at the same time point. (C) Location of proliferating cells within cysts grown for 8 days in collagen. Ten cysts per sample were scored for each condition in each of two independent experiments. Mean \pm s.e.m. of independent experiments. * P <0.05 by two-tailed t -test comparing the percentages of centrally proliferating cells in WT and ZO-1 KD cysts. (D) The lumens of mature cysts grown in Matrigel were loaded with Lucifer Yellow (LY). Left, pseudocolor images reflecting the fluorescence intensity over time are shown. Scale bar: 50 μ m. Loss of fluorescence intensity from the central plane was determined for at least three cysts in each of three independent experiments. Right, mean \pm s.e.m. values for each lumen were determined for WT (n =9) and ZO-1 KD cysts (n =30). P <0.05 by two-tailed t -test, compared to WT at all time points >40 min. TRD, Texas-Red-dextran. (E) Cyst morphology before (left) and after (right) 2 h in hypotonic solution. Dotted red lines indicate the outline of the luminal surface before and after swelling. The percentage increase in luminal area in the central plane was determined; mean \pm s.e.m. of three independent experiments, each in triplicate. * P <0.05 using two-tailed t -test.

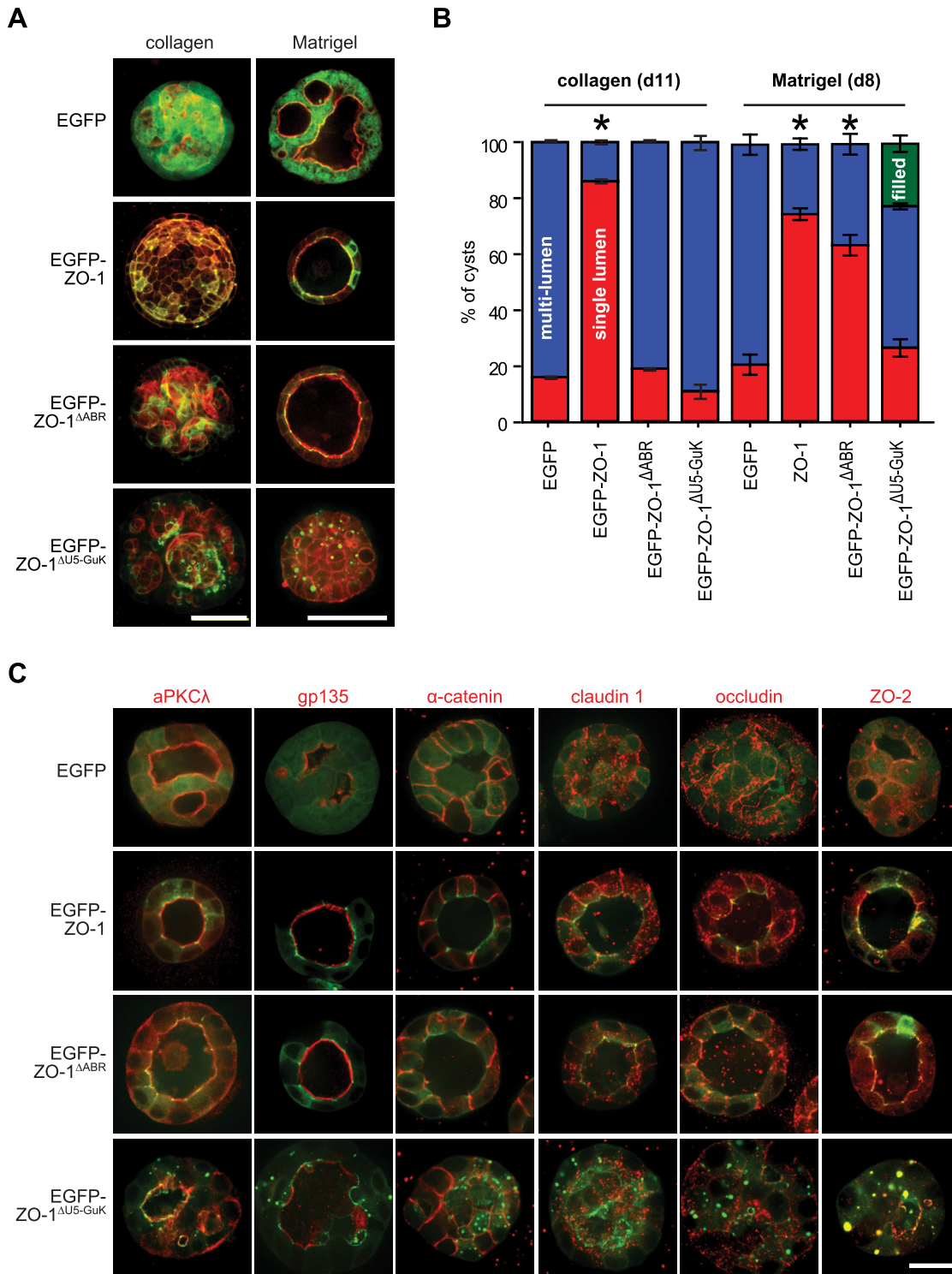


Fig. 4. Morphogenesis requires ZO-1 ABR- and U5-GuK-mediated interactions. (A) Cells expressing EGFP or EGFP-ZO-1 mutants were grown in either collagen or Matrigel to form cysts. Representative images of mature cysts in each culture condition are shown. EGFP, green; F-actin, phalloidin, red. Scale bars: 50 μ m. (B) The lumen phenotype was classed as filled (green), multiple (blue) or single (red) in >100 cysts for each genotype. The mean \pm s.e.m. of three independent experiments is shown. * P <0.05 by two-tailed t -test comparing the single-lumen phenotype of cysts expressing ZO-1 or ZO-1 mutants to those expressing free EGFP. (C) EGFP-, EGFP-ZO-1 or EGFP-ZO-1-mutant-expressing cysts were grown in Matrigel for 4 days and immunostained for aPKC λ , gp135, α -catenin, claudin-1, occludin and ZO-2 (all shown in red) to assess polarization and tight junction organization. EGFP, green. Scale bar: 20 μ m.

2D culture results and indicating that shroom2 is dispensable with respect to lumen formation.

The majority of α -catenin-deficient cells formed unusual sheet-like structures with a single lumen and large tubules extending from

the main body when grown in collagen (Fig. 6D–F). Based on the heterogeneity of cyst morphology after 11 days in culture, we hypothesize that these sheet-like structures begin as hollow cysts that extend tubules before forming single lumen sheet-like

structures (Fig. 6F). In contrast, nearly all α -catenin-deficient cells formed well-polarized spherical cysts with a single hollow lumen when grown in Matrigel (Fig. 6D,E). α -catenin is therefore necessary for the maintenance of spherical cyst shape in the absence of strong external polarity cues but is dispensable with respect to single-lumen formation in either substrate.

ZO-1 interactions with occludin are necessary for tight junction barrier regulation (Buschmann et al., 2013; Raleigh et al., 2011). ZO-1–occludin interactions have not, however, been assessed with respect to morphogenesis. Like ZO-1 KD cells, occludin KD cells formed multi-lumen cysts in both collagen and Matrigel (Fig. 6D, E). Together with the established interaction between the ZO-1 U5-

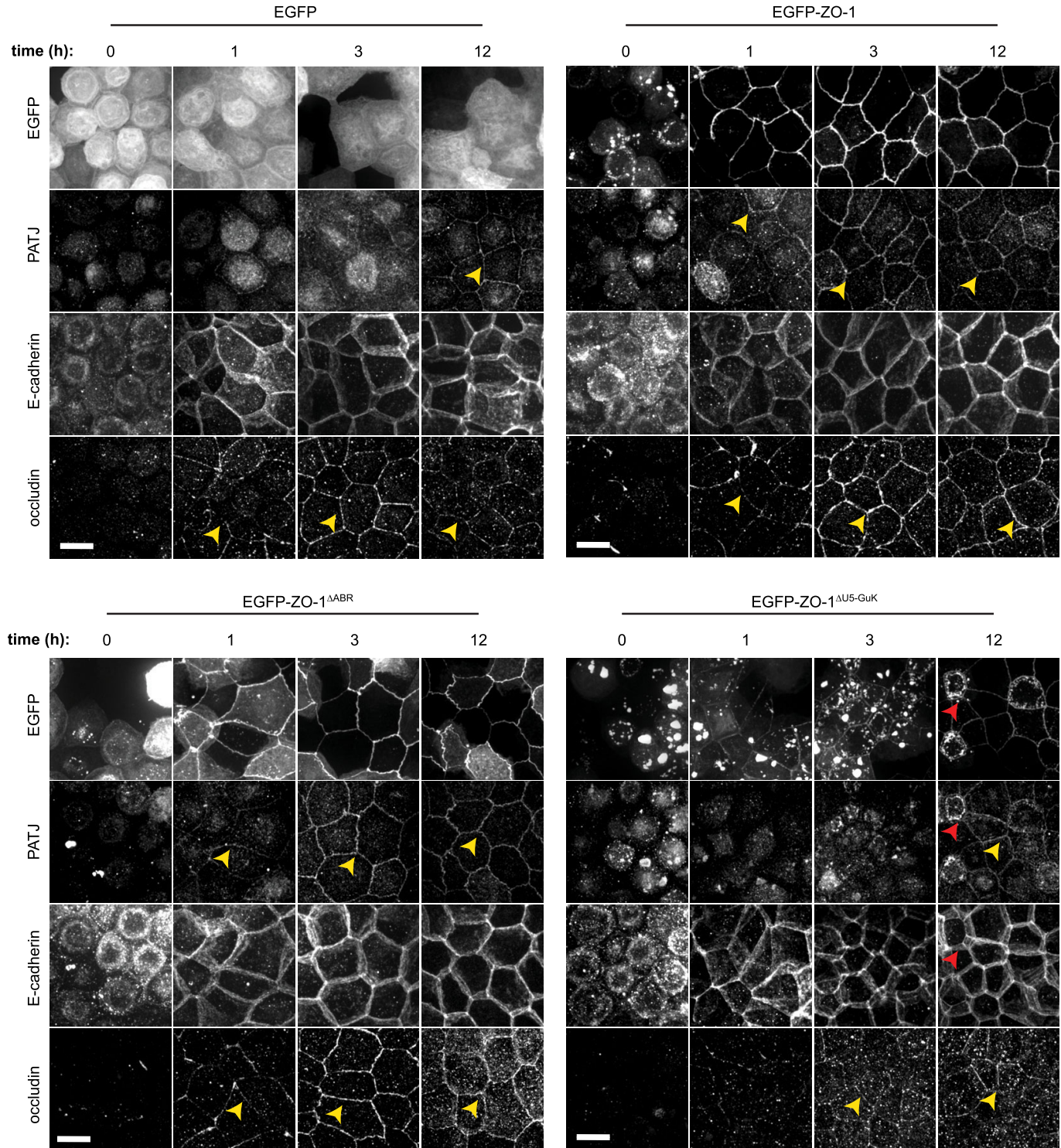


Fig. 5. The ZO-1 U5-GuK domain is necessary for tight junction assembly in 2D cultures. ZO-1 KD cells expressing EGFP-ZO-1 mutants were subjected to the Ca^{2+} -switch assay and stained for either PATJ and E-cadherin or occludin at the indicated time points. Full monolayer thickness maximal projections are shown and are representative of three independent experiments per condition. Yellow arrowheads denote protein recruitment to tight junctions, and red arrowheads indicate cells with high expression levels of EGFP-ZO-1^{ΔU5-GuK}. Scale bars: 10 μm. Additional images are shown in Fig. S3D.

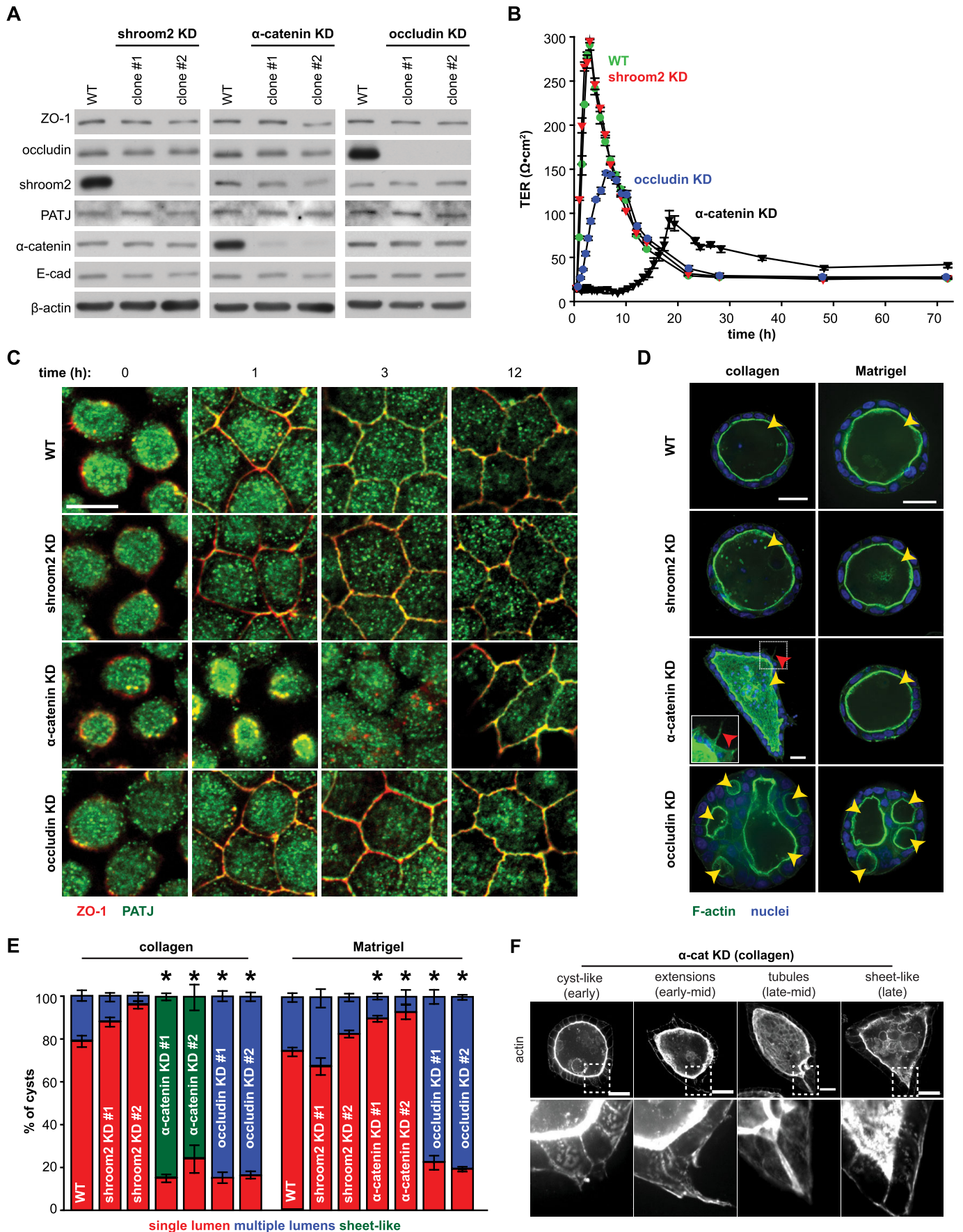


Fig. 6. See next page for legend.

Fig. 6. ZO-1 U5-GuK domain binding partners contribute to protein trafficking and morphogenesis in 2D and 3D cultures. (A) Protein lysates from confluent WT, shroom2 KD, α -catenin KD and occludin KD monolayers derived from the indicated clones were immunoblotted for ZO-1, occludin, shroom2, PATJ and α -catenin. E-cadherin (E-cad) and β -actin were probed as loading controls. Data are representative of three independent experiments. (B) Development of TER in WT, shroom2 KD, α -catenin KD and occludin KD monolayers after Ca^{2+} repletion. The mean \pm s.e.m. from one experiment is shown, representative of three similar studies, each performed in triplicate. (C) Monolayers were immunostained for ZO-1 (red) and PATJ (green) at the indicated times after Ca^{2+} repletion. Representative images from three independent experiments are shown. Scale bar: 10 μm . Grayscale images of each channel are shown in Fig. S4B. (D) Cysts grown from WT, shroom2 KD, α -catenin KD and occludin KD cells in either collagen or Matrigel were stained for F-actin (green, phalloidin) and nuclei (blue, Hoechst 33342). Yellow arrowheads denote lumens, and red arrowheads denote F-actin protrusions from the basal surface of α -catenin KD structures in collagen gel. Representative images from three independent experiments are shown. Scale bars: 25 μm . (E) Lumen phenotypes of mature cysts under each culture condition (collagen or Matrigel) were classified as single lumen (red), multi-lumen (blue) or sheet-like (green). The mean \pm s.e.m. of >100 cysts from each of at least three independent experiments per condition are given. * $P < 0.05$ by two-tailed t -test comparing the percentage of single-lumen WT versus KD cysts under a given culture condition. (F) α -catenin KD cysts were grown in collagen gels for 11 days and stained for F-actin. Images demonstrate the heterogeneity in the 3D structures formed from α -catenin (α -cat) KD cells and are arranged from left to right as an interpretation of sequential progression from spherical cysts, to cysts with extensions, to cysts with tubules, and finally, sheet-like structures. Insets show F-actin accumulation at basal protrusions. Scale bars: 25 μm .

GuK region and occludin, the striking similarity of lumen phenotypes between cysts grown from ZO-1 KD and occludin KD cells suggests that the interaction between ZO-1 and occludin is necessary for single lumen morphogenesis. Further, this indicates that ZO-1 and occludin might act through similar mechanisms to control single epithelial lumen formation.

Occludin and ZO-1 both drive epithelial polarization and orient mitosis to promote single lumen formation

Our 2D analyses showing delayed occludin and PATJ recruitment to cell junctions in ZO-1-deficient monolayers indicate a polarization defect in these cells. Like WT cells, both ZO-1 KD and occludin KD cysts sorted the polarity protein aPKC λ to the luminal surface, where it colocalized with F-actin (Fig. 7A). Consistent with a polarization defect, the orientation of condensed metaphase chromatin relative to the luminal surface differed between WT and KD cells when grown in 3D (Fig. 7A). Orientation of cell division is an early sign of polarization, and previous work has shown that recruitment of a complex comprising NuMA and LGN (also known as GPSM2) to the lateral cortex is required for cell orientation during mitoses in both chick neuroepithelium *in vivo* and MDCK cells *in vitro* (Peyre et al., 2011; Zheng et al., 2010). Further, the NuMA–LGN complex recruits Par1b to define lumen position (Lázaro-Diéguez et al., 2013). To better determine whether knockdown of ZO-1 and occludin was inducing a multi-lumen phenotype through similar mechanisms, we assessed NuMA localization during cell division with epithelial cysts. NuMA localized to the mitotic spindle poles of dividing cells in MDCK cysts (Fig. 7A). Although NuMA was still recruited to spindle poles in ZO-1 or occludin KD cysts, these sites were misoriented with respect to the cyst lumen (Fig. 7A). This suggests that NuMA recruitment is intact in the absence of ZO-1 or occludin, but that overall polarity of spindle orientation and mitosis is disrupted by deletion of either protein.

To better characterize the mitotic polarity defects in ZO-1 and occludin KD cysts, we assessed mitotic spindle orientation using live imaging of cells expressing Lifeact–GFP and H2B–mCherry,

which decorate F-actin (Riedl et al., 2008) and chromatin, respectively. These markers were used to define a plane at the luminal surface between two dividing cells and a line connecting the two sets of chromosomes at anaphase. This angle is 0° when dividing cells are oriented parallel to the luminal surface (Fig. 7B). As expected, this process was tightly controlled in WT cysts, with the majority of divisions within 15° of 0° (in either direction) and a median of $7.7^\circ \pm 2.2^\circ$ (\pm median absolute deviation) (Fig. 7C,D; Movie 1). In contrast, orientation of cell division was markedly disrupted in ZO-1 and occludin KD cysts, with 60% of divisions greater than 15° of the luminal surface and >30% occurring at angles over 30° for both ZO-1 KD (Fig. 7C,D; Movie 1) and occludin KD cells (Fig. 7C,D). Median orientations were $17.0^\circ \pm 4.2^\circ$ and $16.7^\circ \pm 2.9^\circ$ for ZO-1 or occludin KD cysts, respectively. Taken together, these data indicate that ZO-1 and occludin are both required for the earliest phases of polarization within multicellular epithelial structures. Further, these data suggest that ZO-1–occludin interactions regulate this polarization, and that lack of either partner results in defective spindle orientation and multi-lumen cyst development.

Full-length, but not ZO-1-binding defective, occludin restores single lumen formation

The phenotypic similarities between ZO-1 and occludin KD cysts, as well as the failure of ZO-1^{ΔU5-GuK}, which cannot bind to occludin, to rescue these defects strongly suggest that the binding interaction between these two proteins is essential for epithelial polarization, spindle orientation and single-lumen cyst development. We therefore questioned whether an occludin mutant lacking the coiled-coil ZO-1-binding domain OCEL was able to restore these processes (Fig. 8A,B). Because previous studies have linked defective mitotic spindle orientation directly to the multi-lumen phenotype (Durgan et al., 2011; Hao et al., 2010; Jaffe et al., 2008; Qin et al., 2010; Rodriguez-Fraticelli et al., 2010; Xia et al., 2015; Zheng et al., 2010), we relied on the strong phenotype of single- versus multi-lumen cyst formation as both a morphogenetic indicator and marker of early polarization processes – e.g. spindle orientation.

Expression of EGFP–occludin in occludin KD epithelia more than doubled the number of single-lumen cysts that formed, with an increase of $117\% \pm 12\%$ (Fig. 8C,D). In contrast, expression of EGFP–occludin^{ΔOCEL}, which cannot bind to ZO-1 (Li et al., 2005), increased single-lumen formation minimally ($16\% \pm 1\%$). The ZO-1-binding OCEL domain of occludin is therefore necessary for single-lumen formation. The development of single-lumen cysts indicates that preceding processes, including spindle orientation, are corrected by occludin that can bind ZO-1 but not by occludin that cannot. Together with the failure of ZO-1^{ΔU5-GuK} to correct single-lumen formation, these data show that occludin and ZO-1 regulate epithelial polarization through direct interactions with one another.

DISCUSSION

How epithelial tissues form and maintain organized structures with solitary lumens is a fundamental question. Although the substrate that cells are cultured in regulates some aspects of lumen formation, cell-intrinsic factors also impact the ability of epithelia to establish and maintain polarity (Bryant and Mostov, 2008). This is demonstrated by a number of described cell lines that fail to form single-lumen cysts, even when cultured in the presence of strong external polarization cues (Bryant and Mostov, 2008). Herein, we report that ZO-1 is a cell-intrinsic determinant of epithelial polarization and lumen formation through coordination of

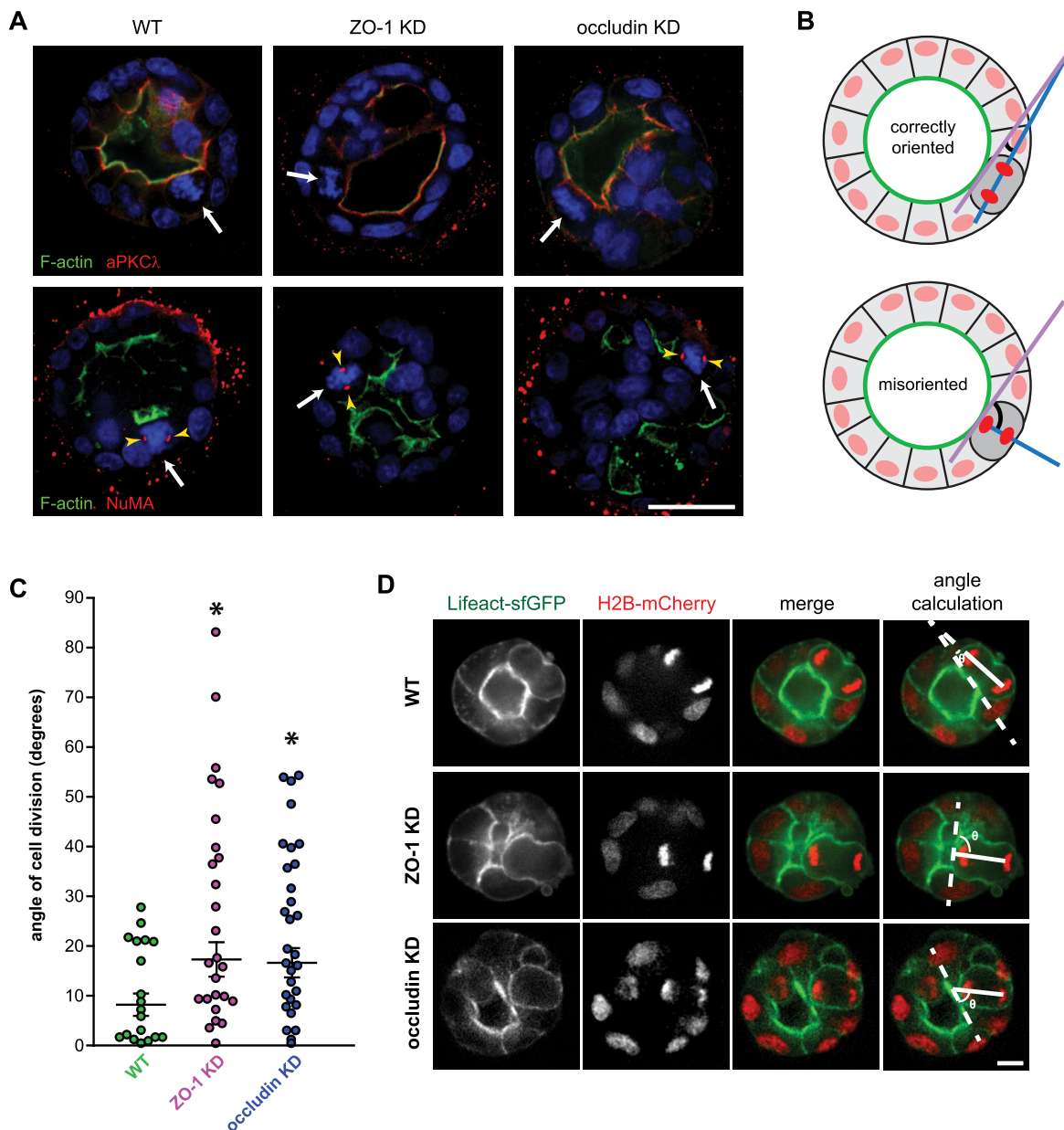


Fig. 7. Occludin and ZO-1 orient mitosis to promote single lumen formation. (A) WT, ZO-1 KD and occludin KD cysts were grown in Matrigel for 4–6 days and stained for nuclei (blue, Hoechst 33342), F-actin (green, phalloidin) and either aPKC λ (red, top panels) or NuMA (red, bottom panels). White arrows depict condensed metaphase chromatin, and yellow arrowheads indicate NuMA localization at mitotic spindle poles. Scale bar: 25 μ m. (B) Method of angle calculation relative to the luminal surface (depicted in green) in a correctly oriented (top) and misoriented (bottom) division event. The magenta line demarcates a plane tangential to the luminal surface, and the blue line indicates a vector between daughter nuclei (red). Black arcs indicate the calculated angle of cell division. (C) Orientation of cell division for WT ($n=19$), ZO-1 KD ($n=26$) and occludin KD ($n=30$) cells. Brackets depict median \pm median absolute deviation. * $P<0.05$ by two-tailed t -test compared to WT. (D) Orientation of cell division was observed in WT, ZO-1 KD and occludin KD cysts expressing Lifeact–sfGFP (green, F-actin) and H2B–mCherry (red, chromatin) by performing live imaging. Representative images of cysts immediately after a cell division event are shown. Right-most images depict the methodology of angle calculation in which the dotted line demarcates the luminal surface and the solid line indicates a vector between daughter nuclei. Scale bar: 10 μ m.

multiple cellular processes, including mitotic spindle orientation. Further, we implicate a specific interaction between ZO-1 and occludin in this process.

Defective spindle orientation was evident in 3D cultures of either ZO-1 KD or occludin KD cells. This is profound given that orientation within the plane of an epithelium contributes to epithelial homeostasis and organogenesis. In fact, many cell lines now known to misorient mitotic spindles during 3D morphogenesis were initially characterized as polarizing slowly, a phenotype that

we also observed in ZO-1-deficient monolayers (Jaffe et al., 2008; Martín-Belmonte et al., 2008; Qin et al., 2010). During mitosis, dividing cells undergo cortical actin reorganization to assume a characteristic rounded morphology. This is thought to anchor both intracellular components of the mitotic machinery, such as the dynein–dynactin motor complex, through astral microtubules and to provide a means of communication with the neighboring environment to control spindle polarization within the plane of an epithelial tissue (Lancaster and Baum, 2014). Studies in both model

organisms and mammalian cell lines conclude that multiple regulators of the actin cytoskeleton, such as Rho kinases, Cdc42 and ERM-family proteins, are necessary for correct spindle orientation (Jaffe et al., 2008; Kunda et al., 2008; Nakajima et al., 2013; Yu et al., 2003). Studies in both *Drosophila* and mammalian cells also indicate that specific basolateral junctional proteins help to polarize cell division, raising the possibility that cell–cell junctions can cooperate with the cortical cytoskeleton to transmit external forces to orient cell division (den Elzen et al., 2009; Nakajima et al., 2013; Tuncay et al., 2015). Interestingly, the prototypical adherens junction protein E-cadherin is necessary for both mitotic orientation within confluent MDCK monolayers and for ZO-1 recruitment to tight junctions during epithelial development (Capaldo and Macara, 2007; den Elzen et al., 2009; Rajasekaran et al., 1996). Together with our results, these data suggest that tight and adherens junctions cooperate to guide polarization of the mitotic spindle.

The junctional protein ZO-1 might orient cell division through its effect on cortical actin organization. Indeed, studies of cells that lacked both ZO-1 and ZO-2 indicate that these proteins, and specifically the ZO-1 U5-GuK region, are necessary for cortical actin organization (Fanning et al., 2012; Ikenouchi et al., 2007; Rodgers et al., 2013). This function of the U5-GuK region could explain the absolutely essential role we report for the U5-GuK region in both tight junction formation and epithelial morphogenesis. The effect must, however, be more complex given that the U5-GuK region does not bind to actin. Alternatively, one could propose that the essential function of the U5-GuK region stems from its requisite role in targeting ZO-1 to the tight junction. This, however, cannot explain the correlation of the severity of the 2D polarization defect with the magnitude of ZO-1^{ΔU5-GuK} expression. It is, therefore, most likely that ZO-1^{ΔU5-GuK} regulates proteins that bind to other ZO-1 domains. Potential effectors include PATJ, which binds to ZO-1 through ZO-3 and claudin-1 in a manner that has been proposed to promote PATJ recruitment to tight junctions (Roh et al., 2002), as well as the transcription factor ZONAB (also known as YBX3) and the Cdc42 guanine nucleotide exchange factor (GEF) tuba (also known as DNMBP), both of which interact directly with ZO-1 (Balda and Matter, 2000; Otani et al., 2006). Consistent with this hypothesis, tuba recruitment to tight junctions is delayed upon ZO-1 depletion, and ZONAB and tuba have both been implicated in 3D morphogenesis through proliferative control and orientation of cell division, respectively (Otani et al., 2006; Sourisseau et al., 2006).

Although the U5-GuK region is essential for setting up a functional tight junction protein network, we also considered the possibility that specific known U5-GuK-mediated interactions are necessary for epithelial morphogenesis. α -catenin depletion markedly delayed tight junction assembly but did not result in the formation of multiple-lumen cysts when grown in 3D cultures. This could reflect the fact that α -catenin KD cells do not have an isolated tight junction defect given that adherens junction assembly was severely disrupted.

Like ZO-1, the U5-GuK binding partner occludin also acts to orient cell division and promotes single lumen formation. However, unlike ZO-1, occludin does not elicit an apparent effect on cortical actin organization or recruitment of tight-junction-associated polarity proteins to the tight junction. Thus, although ZO-1 interactions with F-actin are essential for spindle orientation – i.e. multi-lumen cysts form when ZO-1^{ΔABR} cysts are grown in collagen gels – such interactions cannot fully explain the data presented here. One other factor that could be considered is tissue tension, which

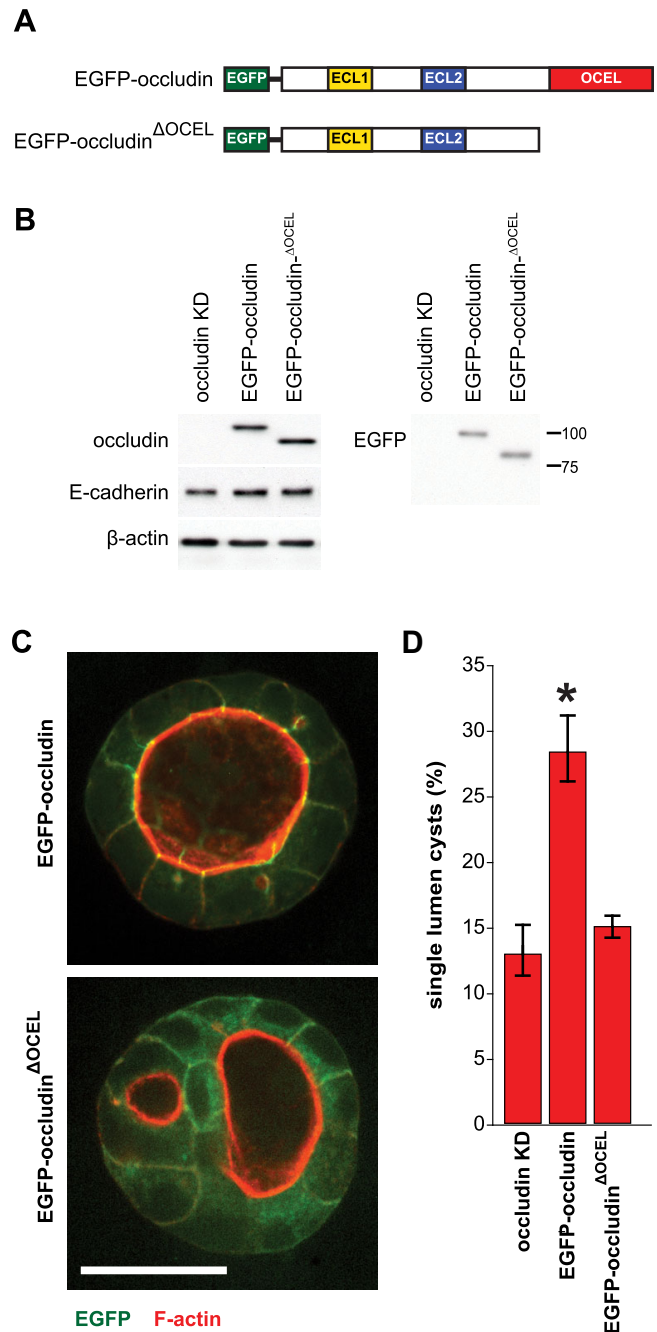


Fig. 8. The occludin interaction with ZO-1 is necessary for single-lumen formation. (A) Domain structure of EGFP-occludin and EGFP-occludin lacking the ZO-1-binding coiled-coil OCEL domain (EGFP-occludin^{ΔOCEL}). ECL, extracellular loop. (B) Occludin KD cells and occludin KD cells that expressed either EGFP-occludin or EGFP-occludin^{ΔOCEL} were grown to confluence, and occludin KD and transgene expression was confirmed by immunoblotting lysates for occludin and EGFP. E-cadherin and β -actin were used as loading controls. (C) Occludin KD cells expressing either EGFP-occludin or EGFP-occludin^{ΔOCEL} were grown for 4–6 days in Matrigel and stained for F-actin (red, phalloidin). Scale bar: 25 μ m. (D) The lumen phenotype of mature cysts expressing either EGFP-occludin or EGFP-occludin^{ΔOCEL} was scored as being a single or multiple lumen for >100 cysts in three independent experiments, each in triplicate. Mean \pm s.e.m. of the percentage of single-lumen cysts in three independent experiments. * P <0.05 by two-tailed t -test compared to occludin KD.

has been proposed to be a determinant of spindle orientation within epithelia. Regulation of tension in an epithelial cyst is likely to require consistent luminal pressure in addition to regulation of

cortical actin. Our studies indicate that ZO-1 depletion results in diminished epithelial barrier function and a macromolecular barrier defect, a finding that is consistent with previously published data in 2D cultures (Van Itallie et al., 2009). Similar barrier defects have been observed upon occludin loss in 2D cultures, and a direct interaction between ZO-1 and occludin has been implicated in barrier regulation during homeostasis and in response to pathogenic stimuli (Buschmann et al., 2013; Marchiando et al., 2010; Raleigh et al., 2011; Van Itallie et al., 2010; Yu et al., 2005a). Our data support a model in which occludin recruitment to the tight junction, and tight junction assembly itself, is downstream of ZO-1 recruitment, as ZO-1 knockdown delayed occludin recruitment, but occludin knockdown did not delay ZO-1 recruitment, to junctions. One could therefore speculate that loss of ZO-1–occludin interactions prevents development of luminal pressure and eliminates the physical force that promotes mitotic spindle orientation. This idea is supported by our observation that ZO-1 and occludin both orient cell division and regulate the paracellular barrier to macromolecular flux. We did assess the effect of increased luminal tension on mature multi-lumen cysts; however, it remains possible that increased luminal pressure could partially correct spindle orientation defects in ZO-1 or occludin KD epithelia. This, however, is unlikely to be the entire explanation for the defects we report, given the genesis of predominantly single-lumen cysts when ZO-2 and ZO-1 were both depleted. Further work is therefore needed to test the hypothesis that the tight junction barrier contributes to maintenance of global tissue forces that direct spindle orientation and overall morphogenesis of epithelium-lined hollow organs.

Our observations are also consistent with the *in vitro* observation that occludin loss in transformed cells leads to failure of epithelial morphogenesis and development of complex multilayered epithelial structures in 2D culture (Li and Mrsny, 2000). Other studies have shown that extrusion of apoptotic cells is ineffective in occludin-deficient epithelia (Yu et al., 2005a) and that occludin KD epithelia fail to correctly activate Rho signaling and remodel actin structure in response to stress (Yu et al., 2005a). These data further suggest that the tight junction barrier is crucial for the maintenance of global tissue forces that direct spindle orientation and overall morphogenesis of epithelium-lined hollow organs. It is notable that, although occludin-knockout mice do not have an obvious intestinal phenotype (Saitou et al., 2000; Schulzke et al., 2005), these mice do have chronic hypertrophic gastritis, testicular atrophy and male sterility, cerebral calcifications, aberrant salivary gland structure and osteopenia (Saitou et al., 2000). Finally, it is important to recognize that no publications have reported stress responses in occludin-knockout mice, although other work has shown that occludin overexpression within intestinal epithelial cells prevents tumor-necrosis-factor-induced barrier loss and diarrhea *in vivo* (Marchiando et al., 2010).

Another major finding is that the ZO-1 ABR is indispensable for epithelial polarization in the absence of strong external cues. Despite the direct binding of ZO-1 and ZO-2, and therefore transmembrane tight junction proteins through ZO-1–ZO-2 interactions, to the actin cytoskeleton, most studies of the ABR in 2D cultures have identified little or no significant contributions to paracellular barrier function or cortical actin organization (Rodgers et al., 2013; Van Itallie et al., 2009). On the contrary, other studies have demonstrated a regulatory function whereby the ABR stabilizes ZO-1 at the tight junction and is necessary for myosin light chain kinase (MLCK)-dependent ZO-1 trafficking and barrier regulation (Yu et al., 2010). The data here further support a model in which, without the ABR, ZO-1 scaffolding

functions are diminished and ZO-1 is unable to effectively facilitate complex interactions (Shen et al., 2008; Yu et al., 2010). Nevertheless, our results indicate that a direct link with F-actin through the ABR is required for ZO-1 to regulate epithelial morphogenesis in some environments.

In summary, we provide direct experimental evidence that the structural tight junction proteins ZO-1 and occludin orchestrate epithelial lumenogenesis. Our data support a model in which a ZO-1 U5-GuK interaction with the occludin OCEL domain promotes formation of a single lumen by providing the cues necessary for polarization of cell division. The broad application of this result during organ development will be an important future direction. It is also notable that altered expression of both ZO-1 and occludin has been reported in tumors, where complex multi-lumen, or cribriform, morphologies are common. Whether loss of ZO-1- or occludin-dependent single-lumen formation impacts progression of glandular cancers – i.e. adenocarcinomas – remains to be determined. Overall, these data provide a framework for future studies of tight-junction-dependent epithelial morphogenesis.

MATERIALS AND METHODS

Cell lines and plasmids

All cells were derived from the T23 clone and maintained in Dulbecco's modified Eagle's medium (DMEM) with geneticin and puromycin (Barth et al., 1997). ZO-1 KD clone 4D3 was cultured with zeocin (Van Itallie et al., 2009). Occludin KD clones F36 and F52 were cultured with hygromycin B (Yu et al., 2005a). ZO-1/ZO-2 double-KD clones were cultured in T23 medium with zeocin and blasticidin (Fanning et al., 2012). All lines were tested quarterly for mycoplasma.

Human ZO-1 cDNA was mutated to evade targeting by small hairpin (sh) RNA (Van Itallie et al., 2009). ZO-1^{ΔABR} and ZO-1^{ΔU5-GuK} constructs, lacking amino acids 1159–1383 and 591–803, respectively, were cloned downstream of an N-terminal EGFP tag and tet-responsive promoter. Shroom2 KD and α -catenin KD cells were generated using pSUPER shroom2 shRNA 5'-GAGCAGGGAAGGTGGGAAA-3' or pSUPER α -catenin shRNA 5'-GGCTAACAGAGACCTGATA-3' (Maiers et al., 2013).

3D culture

3×10^3 cells in collagen (Advanced BioMatrix, San Diego, CA, USA) were plated onto 96-well plates incubated at 37°C before addition of medium. A thin coat of Matrigel (Corning) was applied to a chambered cover glass (Nalge Nunc International), solidified at 37°C and plated with 2.5×10^3 cells in 2.5% Matrigel.

Cyst permeability and swelling assay

Cysts were grown in Matrigel. At day 10, Phenol-Red-free medium containing 0.5 mM Lucifer Yellow and 1 g of 1.3-kDa Texas-Red–Dextran was added for 16 h. Cultures were then perfused with normal medium (permeability assay) or with medium containing 300 mM sucrose (swelling assay). z-stack images were collected every 10 min for 120 min using a DMI6000 microscope (Leica Microsystems, Wetzlar, Germany) within an enclosure at 37°C under 5% CO₂ with a 40×0.6 NA HCX PlanFluotar objective and a Rolera-EMC2 camera (QImaging, Surrey, British Columbia, Canada). Cross-sectional area and average fluorescence intensity of the lumen was calculated using MetaMorph7 software (Molecular Devices).

Ca²⁺-switch assay

1.5×10^5 cells were plated on a 0.33-cm² surface area of 0.4- μ m-pore Transwell inserts (Corning). After 72 h, monolayers were washed and incubated for 16 h in Ca²⁺-free minimal essential medium containing 10% dialyzed FBS and 15 mM HEPES. This was then replaced with standard DMEM containing Ca²⁺, and the TER was measured using an EVOM instrument (World Precision Instruments).

Immunostaining

Collagen gels were treated with 100 U/ml collagenase type VII (Sigma) for 15 min at 37°C. Both collagen and Matrigel cultures were fixed with 2% PFA for 30 min at room temperature, permeabilized with 0.5% Triton X-100, washed with 100 mM glycine and blocked in 0.2% Triton X-100, 0.1% BSA, 0.05% Tween-20 and 10% normal goat serum in PBS. Monolayers were stained using a similar protocol. Antibodies are given in Table S3.

Stained samples were visualized using a Marianas system equipped (3i, Denver, CO, USA) with Zeiss 40×, NA 1.3 oil immersion objective (cysts) or 100× NA 1.45 oil immersion objective (monolayers) and Evolve10 camera (Photometrics) or a Leica DMI6000 instrument with a 63× NA 1.3 glycerol immersion objective and Retiga EXi Fast 1394 camera (QImaging). Both systems were equipped with CSUX Yokogawa spinning discs.

Quantification of junctional protein localization

Using full-thickness maximum intensity projections and ImageJ, two regions were drawn in each cell, one outside (region #1) and one inside the junction (region #2). The area in pixels (A), and the mean, minimum and maximum pixel intensities (PI) were collected. Background pixel intensity ($P_{BK(G)}$) was taken as the minimum pixel intensity. Total fluorescence intensity was calculated for each region as:

$$\text{Total fluorescence intensity (TFI)} = (A) * (PI_{\text{mean}} - P_{BK(G)}).$$

The junctional fluorescence intensity (FI_{Junction}) was calculated as:

$$TFI_{\text{Region1}} - TFI_{\text{Region2}}.$$

The percentage fluorescence intensity at the tight junction was calculated as:

$$100 * (FI_{\text{Junction}} / TFI_{\text{Region1}}).$$

Orientation of cell division

Cysts were grown as Matrigel overlays for 4 days and imaged using the 63× glycerol immersion objective and CSUX-equipped DMI6000 microscope (described above) with an iXon Ultra 897 camera in a chamber at 37°C under 5% CO₂. z-stacks with 1-μm steps were collected at 5-min intervals. To calculate orientation, the z-stack immediately following division was opened in Imap8 software (BitPlane, Zürich, Switzerland). The surface tool was used to generate a surface from each daughter nucleus; the center position was used to calculate a unit vector between the two daughter nuclei. The oblique slicer tool was aligned tangential to the luminal surface where cell division was occurring. Three points were placed along the aligned oblique slicer tool to define the plane of the luminal surface, and the angle between this plane and the vector between the two daughter nuclei was calculated. Group summary data are presented as median±median absolute deviation.

Western blots

Confluent monolayers were lysed and scraped into non-reducing Laemmli sample buffer, and 15 μg of protein was loaded. SDS-PAGE and transfer to PVDF membrane were as described previously (Wang et al., 2006). Membranes were probed with primary antibodies (Table S3) and horseradish-peroxidase-conjugated secondary antibodies (Cell Signaling). Detection used HyBlot chemiluminescence film (Denville Scientific, South Plainfield, NJ). Band densities were quantified using ImageJ.

Acknowledgements

We thank Drs. Tina van Itallie and Jim Anderson (National Institutes of Health) for sharing plasmids and cell lines as well as for thoughtful discussions. We also thank additional members of the Turner laboratory for their input and thoughtful discussions, specifically Le Shen, Weiqi He and Juanmin Zha. We would also like to thank Vytas Bindokas and the rest of the light microscopy core staff at the University of Chicago. Use of the Marianas microscope and discussions regarding image acquisition and analysis were invaluable to this study.

Competing interests

The authors declare no competing or financial interests.

Author contributions

Conceptualization: M.A.O., N.E.J., J.R.T.; Methodology: M.A.O., N.E.J., Y.W., J.R.T.; Investigation and Validation: M.A.O., W.C., A.B., N.S., N.E.J., Y.W., M.H.W.,

M.M.B., J.R.T.; Resources: M.A.O., J.F., B.M., A.S.F., J.R.T.; Writing – Original Draft: M.A.O., J.R.T.; Writing – Review & Editing: M.A.O., W.C., A.B., N.S., N.E.J., Y.W., M.H.W., M.M.B., R.P., J.F., B.M., A.S.F., J.R.T.; Visualization: M.A.O., W.C., A.B., N.S., N.E.J., J.R.T.; Supervision: J.R.T.; Funding acquisition: M.A.O., J.R.T.

Funding

Support was provided by National Institute of Diabetes and Digestive and Kidney Diseases (F30DK103511 to M.A.O., F32DK094550 to M.M.B. and R01DK61931 and R01DK68271 to J.R.T.); National Institute of Child Health and Human Development (T32HD007009 to M.A.O.); Division of Cancer Prevention, National Cancer Institute (P30CA014599); and the National Center for Research Resources (UL1RR024999). Deposited in PMC for release after 12 months.

Supplementary information

Supplementary information available online at <http://jcs.biologists.org/lookup/doi/10.1242/jcs.188185.supplemental>

References

- Amasheh, S., Meiri, N., Gitter, A. H., Schöneberg, T., Mankertz, J., Schulzke, J. D. and Fromm, M. (2002). Claudin-2 expression induces cation-selective channels in tight junctions of epithelial cells. *J. Cell Sci.* **115**, 4969-4976.
- Bagnat, M., Cheung, I. D., Mostov, K. E. and Stainier, D. Y. R. (2007). Genetic control of single lumen formation in the zebrafish gut. *Nat. Cell Biol.* **9**, 954-960.
- Balda, M. S. and Matter, K. (2000). The tight junction protein ZO-1 and an interacting transcription factor regulate ErbB-2 expression. *EMBO J.* **19**, 2024-2033.
- Barth, A. I. M., Pollack, A. L., Altschuler, Y., Mostov, K. E. and Nelson, W. J. (1997). NH2-terminal deletion of beta-catenin results in stable colocalization of mutant beta-catenin with adenomatous polyposis coli protein and altered MDCK cell adhesion. *J. Cell Biol.* **136**, 693-706.
- Bryant, D. M. and Mostov, K. E. (2008). From cells to organs: building polarized tissue. *Nat. Rev. Mol. Cell Biol.* **9**, 887-901.
- Bryant, D. M., Datta, A., Rodríguez-Fraticelli, A. E., Peränen, J., Martín-Belmonte, F. and Mostov, K. E. (2010). A molecular network for de novo generation of the apical surface and lumen. *Nat. Cell Biol.* **12**, 1035-1045.
- Buschmann, M. M., Shen, L., Rajapakse, H., Raleigh, D. R., Wang, Y., Wang, Y., Lingaraju, A., Zha, J., Abbott, E., McAuley, E. M. et al. (2013). Occludin OCEL-domain interactions are required for maintenance and regulation of the tight junction barrier to macromolecular flux. *Mol. Biol. Cell* **24**, 3056-3068.
- Capaldo, C. T. and Macara, I. G. (2007). Depletion of E-cadherin disrupts establishment but not maintenance of cell junctions in Madin-Darby canine kidney epithelial cells. *Mol. Biol. Cell* **18**, 189-200.
- Cerruti, B., Puliafito, A., Shewan, A. M., Yu, W., Combes, A. N., Little, M. H., Chianale, F., Primo, L., Serini, G., Mostov, K. E. et al. (2013). Polarity, cell division, and out-of-equilibrium dynamics control the growth of epithelial structures. *J. Cell Biol.* **203**, 359-372.
- Colegio, O. R., Van Itallie, C. M., McCreary, H. J., Rahner, C. and Anderson, J. M. (2002). Claudins create charge-selective channels in the paracellular pathway between epithelial cells. *Am. J. Physiol. Cell Physiol.* **283**, C142-C147.
- den Elzen, N., Buttery, C. V., Maddugoda, M. P., Ren, G. and Yap, A. S. (2009). Cadherin adhesion receptors orient the mitotic spindle during symmetric cell division in mammalian epithelia. *Mol. Biol. Cell* **20**, 3740-3750.
- Dietz, M. L., Bernaciak, T. M., Vendetti, F., Kielec, J. M. and Hildebrand, J. D. (2006). Differential actin-dependent localization modulates the evolutionarily conserved activity of Shroom family proteins. *J. Biol. Chem.* **281**, 20542-20554.
- Durgan, J., Kaji, N., Jin, D. and Hall, A. (2011). Par6B and atypical PKC regulate mitotic spindle orientation during epithelial morphogenesis. *J. Biol. Chem.* **286**, 12461-12474.
- Etournay, R., Zwaenepoel, I., Perfettini, I., Legrain, P., Petit, C. and El-Amraoui, A. (2007). Shroom2, a myosin-VIIa- and actin-binding protein, directly interacts with ZO-1 at tight junctions. *J. Cell Sci.* **120**, 2838-2850.
- Fanning, A. S. and Anderson, J. M. (2009). Zonula occludens-1 and -2 are cytosolic scaffolds that regulate the assembly of cellular junctions. *Ann. N. Y. Acad. Sci.* **1165**, 113-120.
- Fanning, A. S., Ma, T. Y. and Anderson, J. M. (2002). Isolation and functional characterization of the actin-binding region in the tight junction protein ZO-1. *FASEB J.* **16**, 1835-1837.
- Fanning, A. S., Little, B. P., Rahner, C., Utepergenov, D., Walther, Z. and Anderson, J. M. (2007). The unique-5 and -6 motifs of ZO-1 regulate tight junction strand localization and scaffolding properties. *Mol. Biol. Cell* **18**, 721-731.
- Fanning, A. S., Van Itallie, C. M. and Anderson, J. M. (2012). Zonula occludens-1 and -2 regulate apical cell structure and the zonula adherens cytoskeleton in polarized epithelia. *Mol. Biol. Cell* **23**, 577-590.
- Furuse, M., Itoh, M., Hirase, T., Nagafuchi, A., Yonemura, S., Tsukita, S. and Tsukita, S. (1994). Direct association of occludin with ZO-1 and its possible involvement in the localization of occludin at tight junctions. *J. Cell Biol.* **127**, 1617-1626.

- Furuse, M., Furuse, K., Sasaki, H. and Tsukita, S. (2001). Conversion of zonulae occludentes from tight to leaky strand type by introducing claudin-2 into Madin-Darby canine kidney I cells. *J. Cell Biol.* **153**, 263-272.
- Hao, Y., Du, Q., Chen, X., Zheng, Z., Balsbaugh, J. L., Maitra, S., Shabanowitz, J., Hunt, D. F. and Macara, I. G. (2010). Par3 controls epithelial spindle orientation by aPKC-mediated phosphorylation of apical Pins. *Curr. Biol.* **20**, 1809-1818.
- Hartsock, A. and Nelson, W. J. (2008). Adherens and tight junctions: structure, function and connections to the actin cytoskeleton. *Biochim. Biophys. Acta* **1778**, 660-669.
- Ikenouchi, J., Umeda, K., Tsukita, S., Furuse, M. and Tsukita, S. (2007). Requirement of ZO-1 for the formation of belt-like adherens junctions during epithelial cell polarization. *J. Cell Biol.* **176**, 779-786.
- Itoh, M., Nagafuchi, A., Moroi, S. and Tsukita, S. (1997). Involvement of ZO-1 in cadherin-based cell adhesion through its direct binding to alpha catenin and actin filaments. *J. Cell Biol.* **138**, 181-192.
- Jaffe, A. B., Kaji, N., Durgan, J. and Hall, A. (2008). Cdc42 controls spindle orientation to position the apical surface during epithelial morphogenesis. *J. Cell Biol.* **183**, 625-633.
- Jesaitis, L. A. and Goodenough, D. A. (1994). Molecular characterization and tissue distribution of ZO-2, a tight junction protein homologous to ZO-1 and the *Drosophila* discs-large tumor suppressor protein. *J. Cell Biol.* **124**, 949-961.
- Katsuno, T., Umeda, K., Matsui, T., Hata, M., Tamura, A., Itoh, M., Takeuchi, K., Fujimori, T., Nabeshima, Y.-i., Noda, T. et al. (2008). Deficiency of zonula occludens-1 causes embryonic lethal phenotype associated with defected yolk sac angiogenesis and apoptosis of embryonic cells. *Mol. Biol. Cell* **19**, 2465-2475.
- Kunda, P., Pellling, A. E., Liu, T. and Baum, B. (2008). Moesin controls cortical rigidity, cell rounding, and spindle morphogenesis during mitosis. *Curr. Biol.* **18**, 91-101.
- Lancaster, O. M. and Baum, B. (2014). Shaping up to divide: coordinating actin and microtubule cytoskeletal remodelling during mitosis. *Semin. Cell Dev. Biol.* **34**, 109-115.
- Lázaro-Díéguez, F., Cohen, D., Fernandez, D., Hodgson, L., van Ijzendoorn, S. C. and Müsch, A. (2013). Par1b links lumen polarity with LGN-NuMA positioning for distinct epithelial cell division phenotypes. *J. Cell Biol.* **203**, 251-264.
- Li, D. and Mrsny, R. J. (2000). Oncogenic Raf-1 disrupts epithelial tight junctions via downregulation of occludin. *J. Cell Biol.* **148**, 791-800.
- Li, Y., Fanning, A. S., Anderson, J. M. and Lavie, A. (2005). Structure of the conserved cytoplasmic C-terminal domain of occludin: identification of the ZO-1 binding surface. *J. Mol. Biol.* **352**, 151-164.
- Lin, H.-H., Yang, T.-P., Jiang, S.-T., Yang, H.-Y. and Tang, M.-J. (1999). Bcl-2 overexpression prevents apoptosis-induced Madin-Darby canine kidney simple epithelial cyst formation. *Kidney Int.* **55**, 168-178.
- Madara, J. L., Barenberg, D. and Carlson, S. (1986). Effects of Cytochalasin D on Occluding Junctions of Intestinal Absorptive Cells: Further Evidence That the Cytoskeleton May Influence Paracellular Permeability and Junctional Charge Selectivity. *J. Cell Biol.* **102**, 2125-2136.
- Maiers, J. L., Peng, X., Fanning, A. S. and DeMali, K. A. (2013). ZO-1 recruitment to alpha-catenin—a novel mechanism for coupling the assembly of tight junctions to adherens junctions. *J. Cell Sci.* **126**, 3904-3915.
- Marchiando, A. M., Shen, L., Graham, W. V., Weber, C. R., Schwarz, B. T., Austin, J. R., II, Raleigh, D. R., Guan, Y., Watson, A. J. M., Montrose, M. H. et al. (2010). Caveolin-1-dependent occludin endocytosis is required for TNF-induced tight junction regulation in vivo. *J. Cell Biol.* **189**, 111-126.
- Martín-Belmonte, F., Gassama, A., Datta, A., Yu, W., Rescher, U., Gerke, V. and Mostov, K. (2007). PTEN-mediated apical segregation of phosphoinositides controls epithelial morphogenesis through Cdc42. *Cell* **128**, 383-397.
- Martín-Belmonte, F., Yu, W., Rodríguez-Fraticelli, A. E., Ewald, A. J., Werb, Z., Alonso, M. A. and Mostov, K. (2008). Cell-polarity dynamics controls the mechanism of lumen formation in epithelial morphogenesis. *Curr. Biol.* **18**, 507-513.
- McNeil, E., Capaldo, C. T. and Macara, I. G. (2006). Zonula occludens-1 function in the assembly of tight junctions in Madin-Darby canine kidney epithelial cells. *Mol. Biol. Cell* **17**, 1922-1932.
- Nakajima, Y., Meyer, E. J., Kroesen, A., McKinney, S. A. and Gibson, M. C. (2013). Epithelial junctions maintain tissue architecture by directing planar spindle orientation. *Nature* **500**, 359-362.
- O'Brien, L. E., Jou, T.-S., Pollack, A. L., Zhang, Q., Hansen, S. H., Yurchenco, P. and Mostov, K. E. (2001). Rac1 orientates epithelial apical polarity through effects on basolateral laminin assembly. *Nat. Cell Biol.* **3**, 831-838.
- Otani, T., Ichii, T., Aono, S. and Takeichi, M. (2006). Cdc42 GEF Tuba regulates the junctional configuration of simple epithelial cells. *J. Cell Biol.* **175**, 135-146.
- Peyre, E., Jaouen, F., Saadaoui, M., Haren, L., Merdes, A., Durbec, P. and Morin, X. (2011). A lateral belt of cortical LGN and NuMA guides mitotic spindle movements and planar division in neuroepithelial cells. *J. Cell Biol.* **193**, 141-154.
- Qin, Y., Meisen, W. H., Hao, Y. and Macara, I. G. (2010). Tuba, a Cdc42 GEF, is required for polarized spindle orientation during epithelial cyst formation. *J. Cell Biol.* **189**, 661-669.
- Rajasekaran, A. K., Hojo, M., Huima, T. and Rodriguez-Boulan, E. (1996). Catenins and zonula occludens-1 form a complex during early stages in the assembly of tight junctions. *J. Cell Biol.* **132**, 451-463.
- Raleigh, D. R., Boe, D. M., Yu, D., Weber, C. R., Marchiando, A. M., Bradford, E. M., Wang, Y., Wu, L., Schneeberger, E. E., Shen, L. et al. (2011). Occludin S408 phosphorylation regulates tight junction protein interactions and barrier function. *J. Cell Biol.* **193**, 565-582.
- Riedl, J., Crevenna, A. H., Kessenbrock, K., Yu, J. H., Neukirchen, D., Bista, M., Bradke, F., Jenne, D., Holak, T. A., Werb, Z. et al. (2008). Lifeact: a versatile marker to visualize F-actin. *Nat. Methods* **5**, 605-607.
- Rodgers, L. S., Beam, M. T., Anderson, J. M. and Fanning, A. S. (2013). Epithelial barrier assembly requires coordinated activity of multiple domains of the tight junction protein ZO-1. *J. Cell Sci.* **126**, 1565-1575.
- Rodríguez-Fraticelli, A. E., Vergarajauregui, S., Eastburn, D. J., Datta, A., Alonso, M. A., Mostov, K. and Martin-Belmonte, F. (2010). The Cdc42 GEF Intersectin 2 controls mitotic spindle orientation to form the lumen during epithelial morphogenesis. *J. Cell Biol.* **189**, 725-738.
- Roh, M. H., Liu, C.-J., Laurinec, S. and Margolis, B. (2002). The carboxyl terminus of zona occludens-3 binds and recruits a mammalian homologue of discs lost to tight junctions. *J. Biol. Chem.* **277**, 27501-27509.
- Saitou, M., Furuse, M., Sasaki, H., Schulzke, J.-D., Fromm, M., Takano, H., Noda, T. and Tsukita, S. (2000). Complex phenotype of mice lacking occludin, a component of tight junction strands. *Mol. Biol. Cell* **11**, 4131-4142.
- Schluter, M. A., Pfarr, C. S., Pieczynski, J., Whiteman, E. L., Hurd, T. W., Fan, S., Liu, C.-J. and Margolis, B. (2009). Trafficking of Crumbs3 during cytokinesis is crucial for lumen formation. *Mol. Biol. Cell* **20**, 4652-4663.
- Schulzke, J. D., Gitter, A. H., Mankertz, J., Spiegel, S., Seidler, U., Amasheh, S., Saitou, M., Tsukita, S. and Fromm, M. (2005). Epithelial transport and barrier function in occludin-deficient mice. *Biochim. Biophys. Acta* **1669**, 34-42.
- Shen, L., Weber, C. R. and Turner, J. R. (2008). The tight junction protein complex undergoes rapid and continuous molecular remodeling at steady state. *J. Cell Biol.* **181**, 683-695.
- Shin, K., Straight, S. and Margolis, B. (2005). PATJ regulates tight junction formation and polarity in mammalian epithelial cells. *J. Cell Biol.* **168**, 705-711.
- Sourisseau, T., Georgiadis, A., Tsapara, A., Ali, R. R., Pestell, R., Matter, K. and Balda, M. S. (2006). Regulation of PCNA and cyclin D1 expression and epithelial morphogenesis by the ZO-1-regulated transcription factor ZONAB/DbpA. *Mol. Cell Biol.* **26**, 2387-2398.
- Spadaro, D., Tapia, R., Jond, L., Sudol, M., Fanning, A. S. and Citi, S. (2014). ZO proteins redundantly regulate the transcription factor DbpA/ZONAB. *J. Biol. Chem.* **289**, 22500-22511.
- Stevenson, B. R., Siliciano, J. D., Mooseker, M. S. and Goodenough, D. A. (1986). Identification of ZO-1: a high molecular weight polypeptide associated with the tight junction (zonula occludens) in a variety of epithelia. *J. Cell Biol.* **103**, 755-766.
- Straight, S. W., Shin, K., Fogg, V. C., Fan, S., Liu, C.-J., Roh, M. and Margolis, B. (2004). Loss of PALS1 expression leads to tight junction and polarity defects. *Mol. Biol. Cell* **15**, 1981-1990.
- Tuncay, H., Brinkmann, B. F., Steinbacher, T., Schürmann, A., Gerke, V., Iden, S. and Ebnert, K. (2015). JAM-A regulates cortical dynein localization through Cdc42 to control planar spindle orientation during mitosis. *Nat. Commun.* **6**, 8128.
- Umeda, K., Ikenouchi, J., Katahira-Tayama, S., Furuse, K., Sasaki, H., Nakayama, M., Matsui, T., Tsukita, S., Furuse, M. and Tsukita, S. (2006). ZO-1 and ZO-2 independently determine where claudins are polymerized in tight-junction strand formation. *Cell* **126**, 741-754.
- Van Itallie, C. M. and Anderson, J. M. (2006). Claudins and epithelial paracellular transport. *Annu. Rev. Physiol.* **68**, 403-429.
- Van Itallie, C. M., Fanning, A. S., Bridges, A. and Anderson, J. M. (2009). ZO-1 stabilizes the tight junction solute barrier through coupling to the perijunctional cytoskeleton. *Mol. Biol. Cell* **20**, 3930-3940.
- Van Itallie, C. M., Fanning, A. S., Holmes, J. and Anderson, J. M. (2010). Occludin is required for cytokine-induced regulation of tight junction barriers. *J. Cell Sci.* **123**, 2844-2852.
- Van Itallie, C. M., Aponte, A., Tietgens, A. J., Gucek, M., Fredriksson, K. and Anderson, J. M. (2013). The N and C termini of ZO-1 are surrounded by distinct proteins and functional protein networks. *J. Biol. Chem.* **288**, 13775-13788.
- Wang, F., Schwarz, B. T., Graham, W. V., Wang, Y., Su, L., Clayburgh, D. R., Abraham, C. and Turner, J. R. (2006). IFN-gamma-induced TNFR2 expression is required for TNF-dependent intestinal epithelial barrier dysfunction. *Gastroenterol* **131**, 1153-63.
- Weber, C. R., Liang, G. H., Wang, Y., Das, S., Shen, L., Yu, A. S. L., Nelson, D. J. and Turner, J. R. (2015). Claudin-2-dependent paracellular channels are dynamically gated. *eLife* **4**, e09906.
- Weis, G. V., Knowles, B. C., Choi, E., Goldstein, A. E., Williams, J. A., Manning, E. H., Roland, J. T., Lapierre, L. A. and Goldenring, J. R. (2016). Loss of MYO5B in mice recapitulates Microvillus Inclusion Disease and reveals an apical trafficking pathway distinct to neonatal duodenum. *Cell. Mol. Gastroenterol. Hepatol.* **2**, 131-157.
- Xia, J., Swiercz, J. M., Bañón-Rodríguez, I., Matković, I., Federico, G., Sun, T., Franz, T., Brakebusch, C. H., Kumanogoh, A., Friedel, R. H. et al. (2015).

- Semaphorin-Plexin Signaling Controls Mitotic Spindle Orientation during Epithelial Morphogenesis and Repair. *Dev. Cell* **33**, 299-313.
- Xu, J., Kausalya, P. J., Phua, D. C. Y., Ali, S. M., Hossain, Z. and Hunziker, W.** (2008). Early embryonic lethality of mice lacking ZO-2, but Not ZO-3, reveals critical and nonredundant roles for individual zonula occludens proteins in mammalian development. *Mol. Cell Biol.* **28**, 1669-1678.
- Yu, W., O'Brien, L. E., Wang, F., Bourne, H., Mostov, K. E. and Zegers, M. M.** (2003). Hepatocyte growth factor switches orientation of polarity and mode of movement during morphogenesis of multicellular epithelial structures. *Mol. Biol. Cell* **14**, 748-763.
- Yu, A. S. L., McCarthy, K. M., Francis, S. A., McCormack, J. M., Lai, J., Rogers, R. A., Lynch, R. D. and Schneeberger, E. E.** (2005a). Knockdown of occludin expression leads to diverse phenotypic alterations in epithelial cells. *Am. J. Physiol. Cell Physiol.* **288**, C1231-C1241.
- Yu, W., Datta, A., Leroy, P., O'Brien, L. E., Mak, G., Jou, T.-S., Matlin, K. S., Mostov, K. E. and Zegers, M. M. P.** (2005b). Beta1-integrin orients epithelial polarity via Rac1 and laminin. *Mol. Biol. Cell* **16**, 433-445.
- Yu, W., Shewan, A. M., Brakeman, P., Eastburn, D. J., Datta, A., Bryant, D. M., Fan, Q.-W., Weiss, W. A., Zegers, M. M. P. and Mostov, K. E.** (2008). Involvement of RhoA, ROCK I and myosin II in inverted orientation of epithelial polarity. *EMBO Rep.* **9**, 923-929.
- Yu, D., Marchiando, A. M., Weber, C. R., Raleigh, D. R., Wang, Y., Shen, L. and Turner, J. R.** (2010). MLCK-dependent exchange and actin binding region-dependent anchoring of ZO-1 regulate tight junction barrier function. *Proc. Natl. Acad. Sci. USA* **107**, 8237-8241.
- Zheng, Z., Zhu, H., Wan, Q., Liu, J., Xiao, Z., Siderovski, D. P. and Du, Q.** (2010). LGN regulates mitotic spindle orientation during epithelial morphogenesis. *J. Cell Biol.* **189**, 275-288.

Supplemental Table 1:

Junctional localization of proteins after calcium switch in ZO-1 KD cells expressing EGFP or EGFP-tagged ZO-1 mutants

Occludin Junctional Fraction

time (h)	1	3	12
EGFP	0.42±0.01*	0.52±0.02*	0.47±0.05
EGFP-FL-ZO-1	0.62±0.05 [#]	0.64±0.03 [#]	0.56±0.04
EGFP-ZO-1 ^{ΔABR}	0.58±0.03 [#]	0.63±0.01 [#]	0.50±0.02
EGFP-ZO-1 ^{ΔU5-GuK}	0.44±0.03*	0.39±0.02* [#]	0.37±0.02* [#]

PATJ Junctional Fraction

time (h)	1	3	12
EGFP	0.25±0.01*	0.32±0.03*	0.37±0.04*
EGFP-FL-ZO-1	0.47±0.02 [#]	0.50±0.03 [#]	0.49±0.02 [#]
EGFP-ZO-1 ^{ΔABR}	0.41±0.02 [#]	0.48±0.03 [#]	0.53±0.03 [#]
EGFP-ZO-1 ^{ΔU5-GuK}	0.29±0.03*	0.31±0.02*	0.24±0.01* [#]

E-cadherin Junctional Fraction

time (h)	1	3	12
EGFP	0.78±0.01	0.84±0.01	0.88±0.01
EGFP-FL-ZO-1	0.82±0.04	0.88±0.02	0.88±0.01
EGFP-ZO-1 ^{ΔABR}	0.84±0.02 [#]	0.86±0.01	0.88±0.02
EGFP-ZO-1 ^{ΔU5-GuK}	0.84±0.02 [#]	0.90±0.02 [#]	0.87±0.02

*, p<0.05 vs. EGFP-FL-ZO-1 at given time point

[#], p<0.05 vs. EGFP at given time point

Supplemental Table 2:

Junctional localization of proteins after calcium switch in cells lacking U5-GuK binding partners

ZO-1 Junctional Fraction

time (h)	1	3	12
WT	0.65±0.02	0.69±0.02	0.67±0.02
occludin KD #1	0.57±0.03*	0.63±0.02*	0.60±0.03*
occludin KD #2	0.64±0.03	0.66±0.02	0.66±0.01
shroom2 KD #1	0.61±0.02	0.68±0.02	0.71±0.02
shroom2 KD #2	0.66±0.02	0.72±0.02	0.73±0.02*

PATJ Junctional Fraction

time (h)	1	3	12
WT	0.37±0.02	0.42±0.02	0.48±0.03
occludin KD #1	0.32±0.02*	0.45±0.01	0.43±0.03
occludin KD #2	0.41±0.03	0.46±0.01	0.46±0.01
shroom2 KD #1	0.35±0.01	0.40±0.03	0.45±0.02
shroom2 KD #2	0.37±0.02	0.43±0.02	0.43±0.01

E-cadherin Junctional Fraction

time (h)	1	3	12
WT	0.75±0.03	0.68±0.02	0.66±0.02
occludin KD #1	0.74±0.03	0.69±0.02	0.64±0.01
occludin KD #2	0.76±0.01	0.70±0.01	0.72±0.01*
shroom2 KD #1	0.71±0.03	0.70±0.03	0.66±0.02
shroom2 KD #2	0.80±0.01	0.74±0.03	0.66±0.01

*, p<0.05 vs. WT at given time point

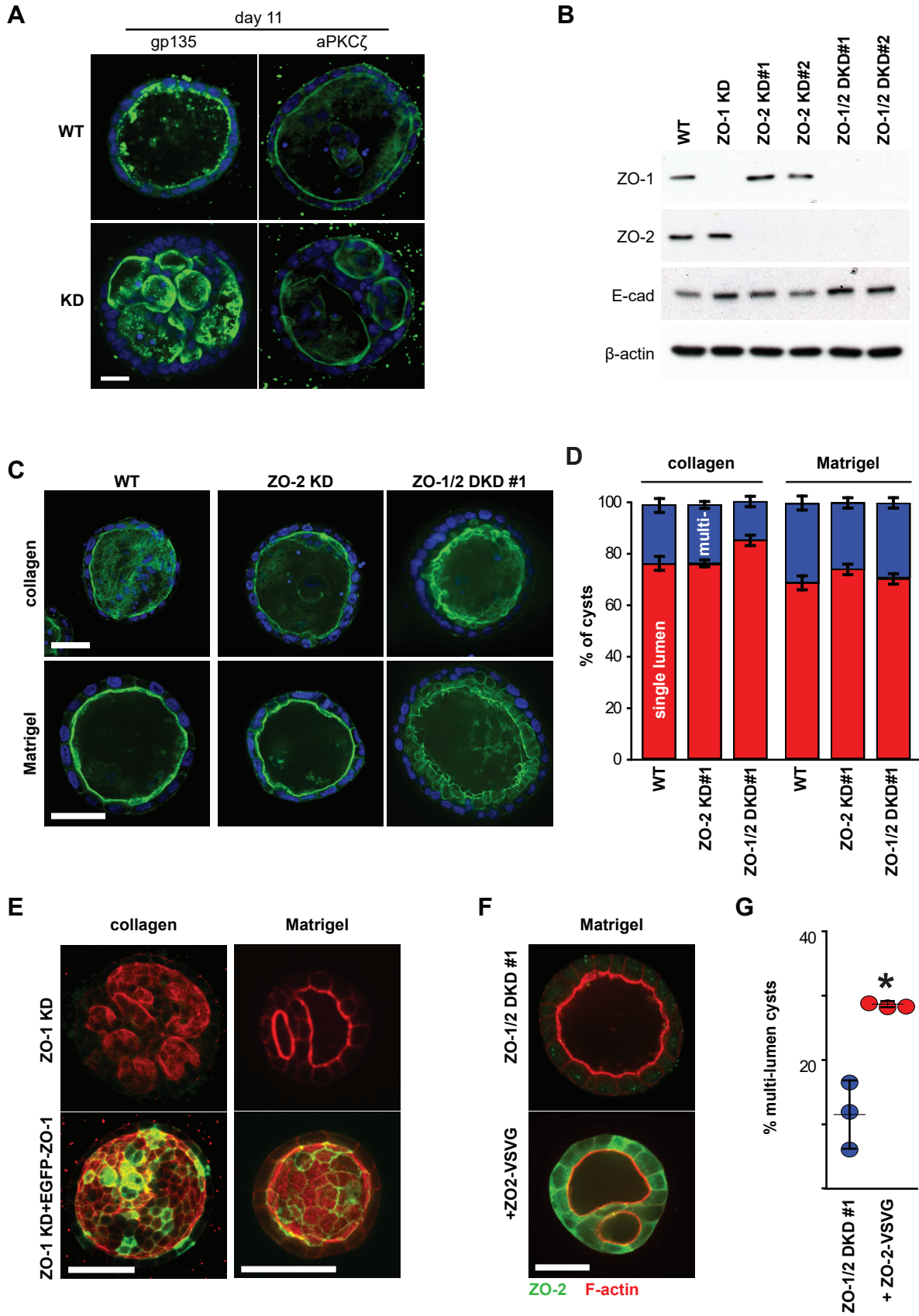
Supplemental Table 3:

Antibodies used:

Antigen	Species	Source	Dilution (IF)	Dilution (WB)
ZO-1	rat	clone R40.76 (culture supernatant, Dan Goodenough, Harvard Medical School)	1:2	1:5
ZO-1	mouse	Invitrogen (33-9100)	1:100	1:1,000
occludin	mouse	Invitrogen (33-1500)	1:100	1:1,000
PATJ	rabbit	Ben Margolis, Univ. Michigan (UM356)	1:100	1:1,000
E-cadherin	rabbit	Cell Signaling (clone 24E10, 3195S)	1:100	1:10,000
E-cadherin	mouse	BD Biosciences (clone 34, 610404)	1:100	N/A
PKC-zeta	rabbit	Sigma-Aldrich (P0713)	1:100	1:1,000
β -actin	mouse	Sigma-Aldrich (clone AC-15, A1978)	N/A	1:10,000
GFP	mouse	Fitch monoclonal antibody core, Univ. Chicago (clone F56-6A.1.2.3)	N/A	1:1,000
Ki67	mouse	Vector Labs (clone SP6, A1978)	1:100	N/A
Cleaved caspase-3	rabbit	Cell Signaling (9664)	1:100	N/A
Shroom2	rabbit	Jeff Hildebrand, Univ. Pittsburgh (UPT115)	1:100	1:1,000
α -catenin	rabbit	Cell Signaling (3236)	1:100	1:1,000
NuMA	rabbit	Abcam (36999)	1:200	N/A
aPKC-lambda	mouse	BD (610207)	1:250	N/A
ZO-2	rabbit	ThermoFisher (38-9100)	1:250	N/A
VSVG	mouse	Sigma (V5507)	1:100	N/A
α -catenin	rabbit	ThermoFisher (71-1200)	1:200	N/A

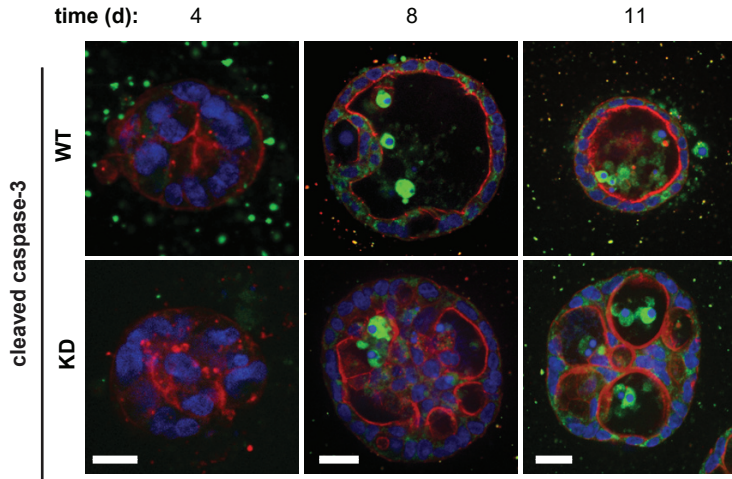
Supplemental Figure 1: The multiple lumen phenotype is specific to ZO-1 loss. A) WT and ZO-1 KD cysts were grown to maturity in collagen and stained for either gp135 (green, left) or aPKC ζ (green, right) and nuclei (blue). Representative images are shown. Bar = 10 μ m. Images are representative of at least 3 independent experiments for each condition, all with similar results.

A previous study reported that ZO-1/ZO-2 double knockdown (DKD) cells are capable of forming single lumen cysts in collagen gels, thereby suggesting that ZO-1 is dispensable for single lumen formation (Fanning et al., 2012). To directly address this potential discrepancy, we tested ZO-1/ZO-2 DKD cells as well as in ZO-2 KD cells in both collagen and Matrigel substrates. B) Western blot for ZO-1 and ZO-2 protein expression in confluent WT, ZO-1 KD, ZO-2 KD, and ZO-1/ZO-2 DKD monolayers. E-cadherin and β -actin were used as loading controls. C) Representative micrographs of mature WT, ZO-2 KD, and ZO-1/ZO-2 KD grown in collagen and Matrigel stained for F-actin (green) and nuclei (blue). In contrast to ZO-1 KD cells, single lumen cysts formed in both ZO-2 KD and ZO-1/ZO-2 DKD cells. Bars = 50 μ m. D) Lumen phenotype of mature WT, ZO-2 KD, and ZO-1/ZO-2 DKD cysts grown in collagen or Matrigel was qualified as multi-lumen (blue) or single lumen (red). Values are mean \pm s.e.m. of >100 cysts from 3 independent experiments per condition. E) EGFP-ZO-1 expression in ZO-1 KD cells restored single lumen formation. Representative images of mature ZO-1 KD cysts and ZO-1 KD cysts expressing EGFP-ZO-1 (shown in green) grown in either collagen or Matrigel. Cysts were stained for F-actin (red). Bars = 50 μ m. Data are representative of at least 3 independent experiments for each condition, all with similar results. F) ZO-2 expression in ZO-1/ZO-2 DKD cells increased numbers of multi-lumen cysts. ZO-2-VSVG was expressed in ZO-1/ZO-2 DKD cells. ZO-1/ZO-2 DKD cells with and without ZO-2-VSVG expression were grown to maturity in Matrigel and stained for ZO-2 (green) and F-actin (red). Representative images are shown. Bar = 25 μ m. G) Lumen phenotype was scored as single or multiple lumens, and the percent of multiple-lumen cysts is shown for ZO-1/ZO-2 DKD cells with (red dots) and without (blue dots) ZO-2-VSVG expression. Individual data points are independent experiments and represent >100 cysts scored for each cell type. Brackets represent mean \pm s.e.m. of 3 independent experiments. *, $p < 0.05$ by two-tailed t-test.

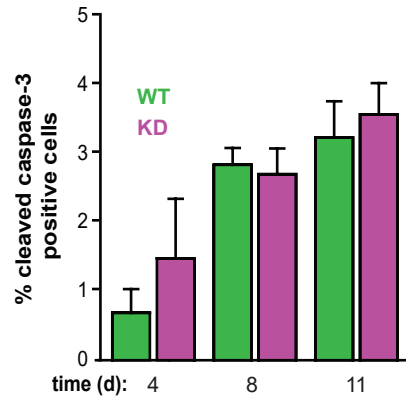


Supplemental Figure 2: ZO-1 is responsible for diverse morphogenetic processes. A) Cysts were grown in collagen and stained for cleaved caspase 3 (green), F-actin (red), and nuclei (blue) at indicated times. Bar = 10 μ m. Images are representative of 3 independent experiments for each condition, all with similar results. B) Thirty cysts of each genotype were scored for cleaved caspase-3 staining. Mean \pm s.e.m from 3 independent experiments. C) WT and ZO-1 KD cells were grown in collagen gels for 18 days and stained for F-actin (red) and nuclei (blue). Bar = 10 μ m. Cysts were classified either single lumen (red) or multi-lumen (blue). Mean \pm s.e.m. of >100 cysts from each of 3 independent experiments. *, p<0.05 by two-tailed t-test comparing percent multi-lumen of WT vs. KD cysts. D) Growth curves of WT and KD monolayers. Reduced serum (2.5%) media was used from day 4 through 6, as indicated. Mean \pm s.e.m. of triplicate samples from an experiment that is representative of 3 independent experiments, all with similar results. *, p<0.05 by two-tailed t-test between WT vs. KD. E) Cysts were grown in collagen gels and fed with media containing either normal (10%) or reduced (2.5%) serum from days 4 through 11. Lumen phenotype was scored as either single (red) or multi-lumen (blue). Mean \pm s.e.m. of >100 cysts in each of 3 independent experiments. *, p<0.05 by two-tailed t-test.

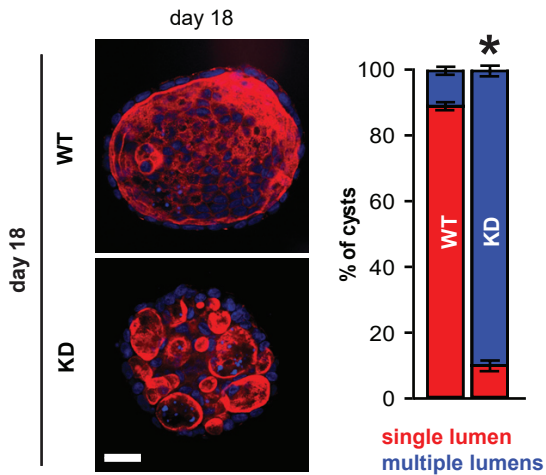
A



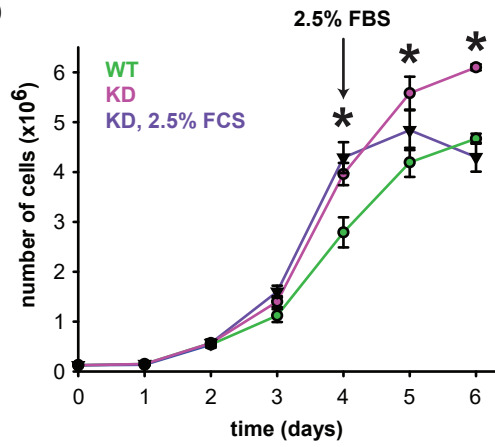
B



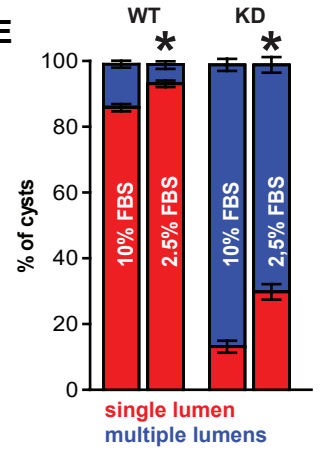
C



D

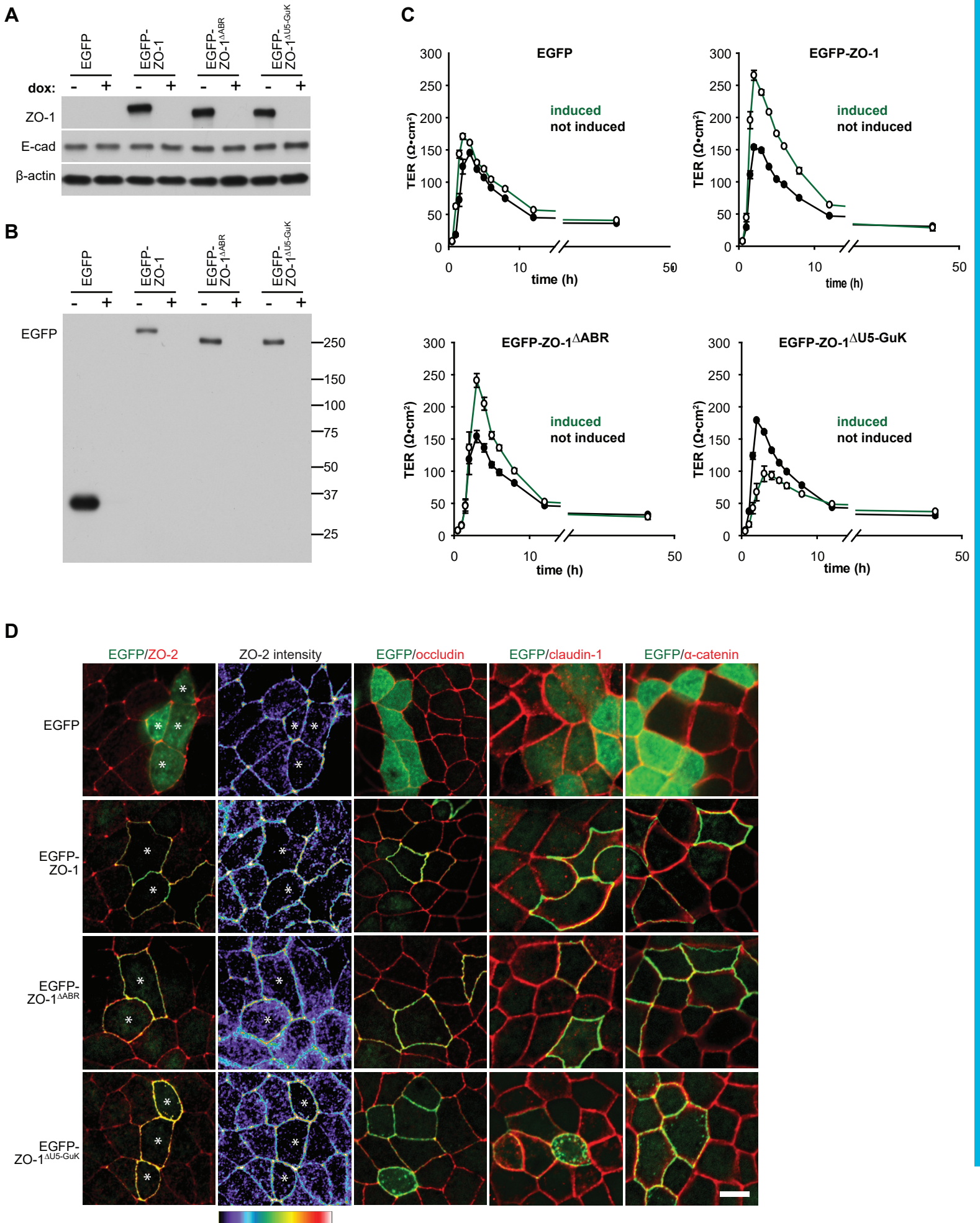


E

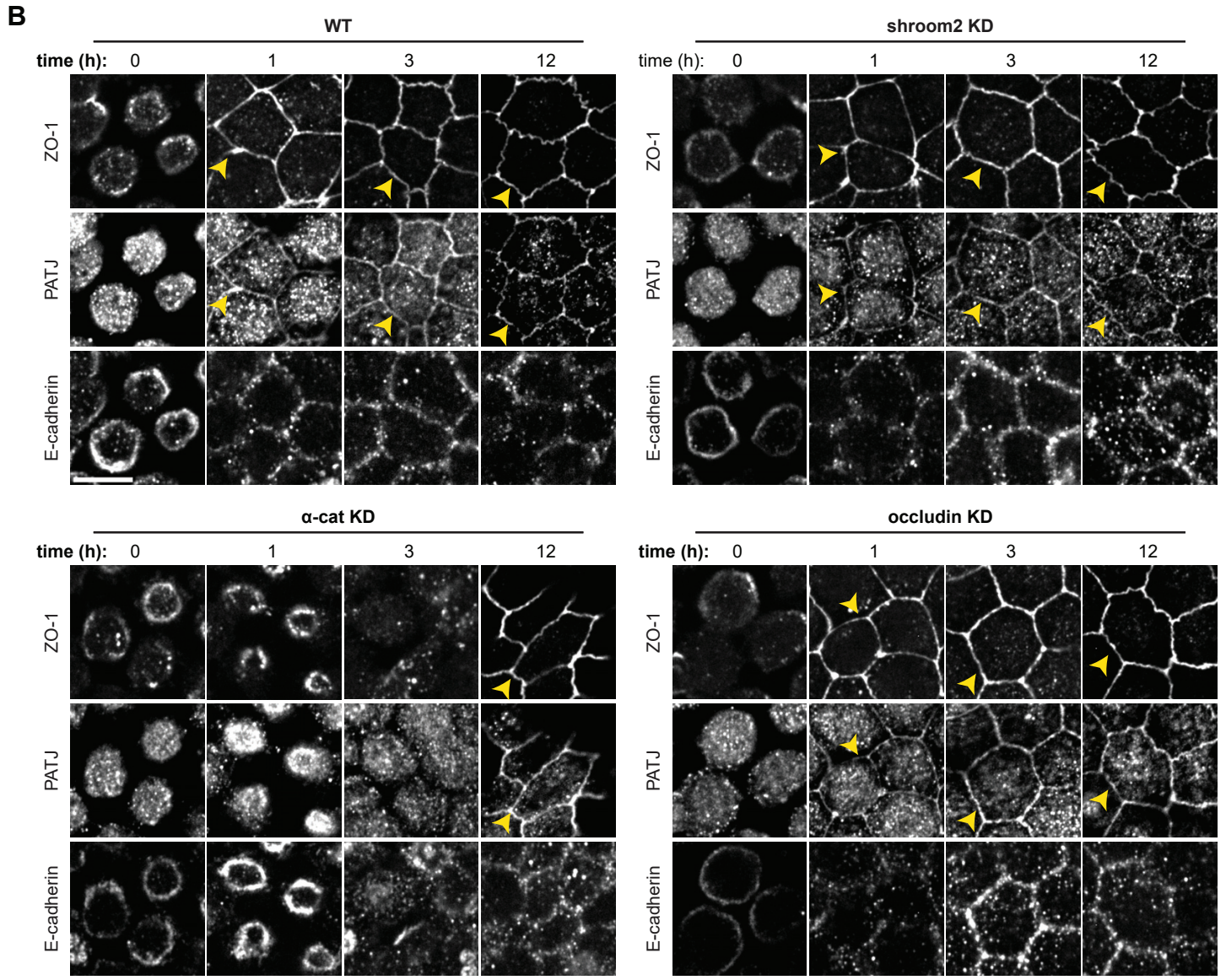
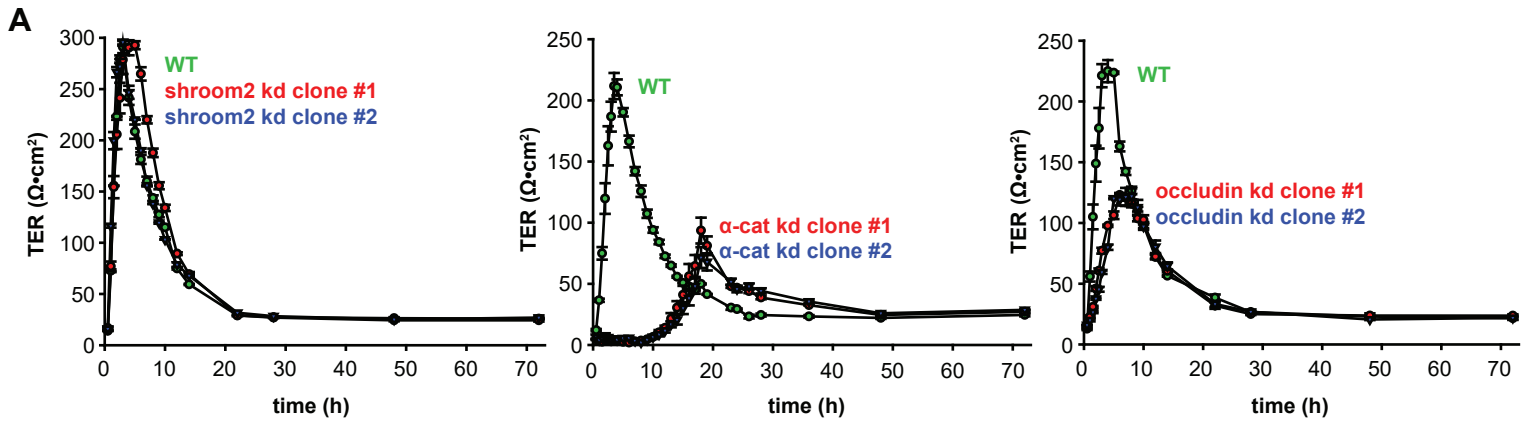


Supplemental Figure 3: Multiple ZO-1 domains are necessary for epithelial morphogenesis and barrier assembly.

A) Inducible expression of EGFP, EGFP-ZO-1, EGFP-ZO-1^{ΔABR}, or EGFP-ZO-1^{ΔU5-GuK} in ZO-1 KD cells was confirmed by western blot. Lysates from confluent monolayers cultured in media with or without doxycycline were probed for ZO-1 to confirm inducible expression of ZO-1 proteins. E-cadherin and β-actin were used as loading controls. Data are representative of at least 3 independent experiments for each condition, all with similar results. B) Expression of EGFP epitope was confirmed by immunoblotting the same lysates as in panel (A) for EGFP. C) TER of monolayers with inducible expression of EGFP-ZO-1 mutants was monitored at indicated times after calcium repletion. Monolayers were cultured in media -dox (green lines) to induce expression or +dox (black lines) to repress expression during barrier development. Mean±s.e.m. are representative of 3 independent experiments, each performed in triplicate. D) EGFP, EGFP-ZO-1, EGFP-ZO-1^{ΔABR}, or EGFP-ZO-1^{ΔU5-GuK} expression was induced in a small proportion of cells within a ZO-1 KD monolayer. Mature monolayers were stained for ZO-2, occludin, claudin-1, and α-catenin (shown in red) 4 days after plating. ZO-2 recruitment to the tight junction was markedly enhanced by expression of EGFP-ZO-1^{ΔU5-GuK}, but not other EGFP-tagged proteins (see pseudocolor intensity images).



Supplemental Figure 4: ZO-1 U5-GuK binding partners orchestrate functional and structural barrier formation. A) TER of WT and 2 independent clones of shroom2 KD, α -catenin KD, and occludin KD monolayers at indicated times after calcium switch. Data for each line are displayed as mean \pm s.e.m. and are representative of 3 independent experiments performed in triplicate (for each line). One representative trace of WT and one clone of each KD cell line were combined to create the traces in Figure 7B. B) WT, shroom2 KD, α -catenin KD, and occludin KD monolayers were immunostained for ZO-1, PATJ, and E-cadherin at indicated times after calcium repletion. Grayscale images are shown. Yellow arrowheads mark areas of PATJ or ZO-1 recruitment to tight junctions. Fluorescence intensities are scaled identically for a given antigen. Merged images are shown in Figure 7C. Images are representative of at least 3 independent experiments for each condition, all with similar results. Bar = 10 μ m.



Supplemental Movie: Mitotic spindle orientation is disturbed in ZO-1 KD cells. Movie shows live imaging of cysts grown from WT (control) and ZO-1 KD (ZO-1 kd) cells expressing Lifeact-sfGFP (green) and H2B-mCherry (red). Arrows indicated mitotic events (movie pauses at these points).

